RESEARCH ARTICLE

Comprehensive evaluation of the Copernicus Atmosphere Monitoring Service (CAMS) reanalysis against independent observations: Reactive gases

Annette Wagner[1,*], Y. Bennouna[2], A.-M. Blechschmidt[3], G. Brasseur[1], S. Chabrillat[4], Y. Christophe[4], Q. Errera[4], H. Eskes[5], J. Flemming[6], K. M. Hansen[7], A. Inness[6], J. Kapsomenakis[8], B. Langerock[4], A. Richter[3], N. Sudarchikova[1], V. Thouret[2], and C. Zerefos[8,9]

The Copernicus Atmosphere Monitoring Service (CAMS) is operationally providing forecast and reanalysis products of air quality and atmospheric composition. In this article, we present an extended evaluation of the CAMS global reanalysis data set of four reactive gases, namely, ozone (O_3), carbon monoxide (CO), nitrogen dioxide (NO_2), and formaldehyde (HCHO), using multiple independent observations. Our results show that the CAMS model system mostly provides a stable and accurate representation of the global distribution of reactive gases over time. Our findings highlight the crucial impact of satellite data assimilation and emissions, investigated through comparison with a model run without assimilated data. Stratospheric and tropospheric O_3 are mostly well constrained by the data assimilation, except over Antarctica after 2012/2013 due to changes in the assimilated data. Challenges remain for O_3 in the Tropics and high-latitude regions during winter and spring. At the surface and for short-lived species (NO_2), data assimilation is less effective. Total column CO in the CAMS reanalysis is well constrained by the assimilated satellite data. The control run, however, shows large overestimations of total column CO in the Southern Hemisphere and larger year-to-year variability in all regions. Concerning the long-term stability of the CAMS model, we note drifts in the time series of biases for surface O_3 and CO in the Northern midlatitudes and Tropics and for NO_2 over East Asia, which point to biased emissions. Compared to the previous Monitoring Atmospheric Composition and Climate reanalysis, changes in the CAMS chemistry module and assimilation system helped to reduce biases and enhance the long-term temporal consistency of model results for the CAMS reanalysis.

1. Introduction

The Copernicus Atmosphere Monitoring Service (CAMS; http://atmosphere.copernicus.eu) is a component of the European Union's Earth Observation Programme Copernicus. This service is designed to meet the needs of policy makers and stakeholders for data and information concerning environmental issues such as climate change, air pollution, and other atmospheric challenges like volcanic eruptions. The CAMS core services include, among others, the daily production of near-real-time (NRT) analyses and forecasts of global atmospheric composition (AC), European air quality products with an ensemble system of regional models, and solar and ultraviolet (UV) radiation products. CAMS is also producing global reanalysis data sets of reactive trace gases, greenhouse gases, and aerosol concentrations. These retrospective analyses of AC are beneficial for air quality and climate studies (e.g., Bechtold et al., 2009; Benedetti et al., 2014), solar spectral irradiance studies (e.g., Mueller and Träger-Chatterjee, 2014; Polo et al., 2017), monitoring of stratospheric composition (e.g.,

[1] Max Planck Institute for Meteorology, Hamburg, Germany

[2] Laboratoire d'Aérologie, Université de Toulouse, CNRS-UPS, Toulouse, France

[3] Institute of Environmental Physics, University of Bremen, Bremen, Germany

[4] Royal Belgian Institute for Space Aeronomy (BIRA-IASB), Uccle, Belgium

[5] Royal Netherlands Meteorological Institute, De Bilt, the Netherlands

[6] European Centre for Medium-Range Weather Forecasts, Reading, UK

[7] Aarhus University, Roskilde, Denmark

[8] Academy of Athens, Athens, Greece

[9] Navarino Environmental Observatory (NEO), Messinia, Greece

* Corresponding author:
Email: annette.wagner@mpimet.mpg.de

Lefever et al., 2015; Errera et al., 2019), or as boundary condition for regional models (e.g., Schere et al., 2012; Giordano et al., 2015; Im et al., 2015). Within the CAMS preparatory project, Monitoring Atmospheric Composition and Climate (MACC), a 10-year reanalysis, was produced (Inness et al., 2013). About 3,000 users have downloaded the MACC reanalysis, which covers the years 2003–2012, since its release in 2013. The MACC reanalysis has not been extended because of major changes in the Integrated Forecasting System (IFS) model configuration (Flemming et al., 2015). After the release of a test reanalysis for reactive gases and aerosols (CAMS Interim Reanalysis; Flemming et al., 2017), the CAMS reanalysis was produced, which covers the years from 2003 onward (Inness et al., 2019). The MACC reanalysis suffered from known inconsistencies in the assimilated data, which led to drifts in carbon monoxide (CO) and ozone (O_3) model fields and limited its use for reliable trend studies.

An important part of the CAMS service is the provision of independent quality assurance information to the CAMS users. A dedicated validation team produces updated evaluations of the CAMS forecast products every 3 months, based on a multitude of independent observational data sets. A description of these validation activities and results are presented in Eskes et al. (2015), Cuevas et al. (2015), and Wagner et al. (2015). During the production of the CAMS reanalysis, a series of validation reports have been produced to monitor the stability of the data sets (Bennouna et al., 2020). All validation reports are publicly available and can be downloaded from the CAMS quality assurance webpages at https://atmosphere.copernicus. eu/quality-assurance. Inness et al. (2019) provide a comprehensive description of the CAMS modeling system used for the CAMS reanalysis and in this context also present selected initial comparisons to observations for the period 2003–2016 in order to demonstrate improvements compared to previous reanalysis runs, that is, the CAMS interim reanalysis (Flemming et al., 2017) and the MACC reanalysis (Inness et al., 2013). Wang et al. (2020) present additional validation results from comparisons with airborne field campaign data for the period 2003–2016. An intercomparison study of tropospheric O_3 reanalysis products based on the same period has been conducted by Huijnen et al. (2020).

This article presents the full evaluation results from the CAMS validation team with independent observational data, covering 16 years of reanalysis (2003–2018). Here, we evaluate the CAMS reanalysis of reactive gases, namely, O_3, CO, nitrogen dioxide (NO_2), and formaldehyde (HCHO). In the present study, the focus is set on the temporal consistency and stability of the model and on the quantification of seasonal and interannual biases. In order to thoroughly assess the impact of data assimilation and the influence of emissions, the results from a separate model run, for which data assimilation has been switched off (further referred to as "control run"), are included and analyzed. Improvements and shortcomings of the CAMS reanalysis compared to the previous MACC reanalysis are likewise quantified and discussed. The article is structured in the following way: Section 2 provides an overview of

the reanalysis model system, the validation data, and methods. Section 3 discusses the validation results, and Section 4 handles the conclusions.

2. Description of the CAMS reanalysis system, validation data, and methods
2.1. The CAMS reanalysis model system
The CAMS reanalysis consists of 3D time-consistent AC fields, including aerosols and chemical species. The meteorological model is based on the IFS cycle 42R1, with interactive O_3 and aerosol feeding its radiation scheme, 60 hybrid sigma/pressure (model) levels in the vertical up to the top level at 0.1 hPa, and a horizontal resolution of approximately 80 km (Inness et al., 2019). For the CAMS reanalysis, IFS includes the modified Carbon Bond 2005 Chemical Mechanism (CB05) tropospheric chemistry scheme (Williams et al., 2013), which was originally developed for the TM5 chemistry transport model (CTM; Huijnen et al., 2010). The model computes stratospheric O_3 using the same Cariolle scheme (Cariolle and Teyssèdre, 2007), as in the meteorological production of IFS, while stratospheric NO_x is constrained through a climatological ratio of HNO_3/O_3 at 10 hPa. Inness et al. (2015, 2019) provide a detailed description of data assimilation for chemical trace gases and Benedetti et al. (2009) for aerosols. **Table 1** lists the data sets used in the assimilation system, and Figure S1 displays a time series for data assimilation in the CAMS reanalysis. Anthropogenic reactive gas emissions are based on MACCity (Granier et al., 2011), where wintertime CO emissions have been scaled up over Europe and the United States (Stein et al., 2014). Monthly mean biogenic emissions are derived from hourly calculations by the Model of Emissions of Gases and Aerosols from Nature (MEGAN) using NASA's Modern-Era Retrospective Analysis for Research and Applications (MERRA) reanalyzed meteorology (Sindelarova et al., 2014). NRT fire emissions are taken from the Global Fire Assimilation System (GFAS) v1.2 (Kaiser et al., 2012). Table S1 lists the major differences between the MACC and CAMS reanalysis data sets. In order to assess the impact of data assimilation, our evaluations also include the CAMS control run. The control run applies the same settings as the CAMS reanalysis, except that data assimilation is switched off. It consists of 24-h cycling forecasts and uses the meteorological fields from the CAMS reanalysis. A more detailed documentation of the CAMS reanalysis model setup can be found on the CAMS Confluence webpage. The CAMS 3D reanalysis products are stored as 3-hourly fields. Data are publicly available from the CAMS Atmosphere Data Store.

2.2. Validation data and metrics
All data sets used in our validations are listed in **Tables 2** and **3**. As we use a wide range of different observations, more comprehensive descriptions of the individual observational data sets and validation algorithms are provided in the supplement (Section S1) and in Eskes et al. (2018). Validation metrics are listed in **Table 4**. More detailed information and a discussion concerning the use of the respective validation metrics can be found in Eskes et al. (2015) and Wagner et al. (2015). **Table 5** lists all acronyms.

Table 1. Overview of the satellite retrievals that are actively assimilated in the CAMS reanalysis. DOI: https://doi.org/10.1525/elementa.2020.00171.t1

Variable	Instrument	Satellite	Product	Origin, period	AK
O_3	SCIAMACHY	Envisat	TC	CCI: 20030101–20120408	No
O_3	MIPAS	Envisat	PROF	ESA NRT: 20030127–20030720	No
				MARS ESA NRT: 20030721–20040326	
				CCI: 20050127–20120331	
O_3	MLS	Aura	PROF	V4: 20040803–20180312	
				V4 NRT: 20180313–	
O_3	OMI	Aura	TC	KNMI V003; reprocessed 20040803–20150531 NRT 20150601–	No
O_3	GOME-2	MetOp-A	TC	CCI BIRA (fv0100): 20070123–20121231	No
				CCI BIRA (fv0300): 201301–201612	
				GDP4.8 ACSAF/DLR: 20170101–20181231	
O_3	GOME-2	MetOp-B	TC	CCI BIRA (fv0300): 201301–201612	No
				GDP4.8 ACSAF/DLR: 20170101–20181231	
O_3	SBUV/2	NOAA-14	PC 13L	NASA v8.6: 200407–200609	No
O_3	SBUV/2	NOAA-16	PC 13 L	NASA v8.6: 200301–200706	No
			21L	20111201–20130708	
				NASA v8.6 NRT: 20130709–201406	
O_3	SBUV/2	NOAA-17	PC 13L	NASA v8.6: 200301–201108	No
O_3	SBUV/2	NOAA-18	PC 13L	NASA v8.6: 200507–201211	No
O_3	SBUV/2	NOAA-19	PC 13 L	NASA v8.6: 200903–20130708	No
			21L	NASA v8.6, NRT: 20130709–20181231	
CO	MOPITT	Terra	TC	V6 (TIR): 2003–2016	Yes
				V7 (TIR): 201701 onward	
NO_2	SCIAMACHY	Envisat	TRC	v1p: 20030101–20101231	Yes
				v2: 20110101–20120409	
NO_2	GOME-2	MetOp-A	TRC	ACSAF GDP4.8: 20070418–20181231	Yes
NO_2	GOME-2	MetOp-B	TRC	ACSAF GDP4.8: 20130101–20181231	Yes
NO_2	OMI	Aura	TRC	COL3: 20041001–20181231	Yes

AK = Averaging Kernel; CAMS = Copernicus Atmosphere Monitoring Service; O_3 = ozone; CO = carbon monoxide; NO_2 = nitrogen dioxide; SCIAMACHY = Scanning Imaging Absorption Spectrometer for Atmospheric ChartographY; MIPAS = Michelson Interferometer for Passive Atmospheric Sounding; MLS = Microwave Limb Sounder; GOME = Global Ozone Monitoring Experiment; SBUV = Solar Backscatter Ultraviolet Radiometer; MOPITT = Measurements of Pollution in the Troposphere; OMI = Ozone Monitoring Instrument.

3. Results and discussion

3.1. Stratospheric ozone

In the stratosphere, O_3 is validated with vertical profile observations from satellites and sondes as well as with partial column observations from the Network for the Detection of Atmospheric Composition Change (NDACC).

Figure 1 shows the results of the evaluation with Michelson Interferometer for Passive Atmospheric Sounding (MIPAS), Microwave Limb Sounder (MLS), and Atmospheric Chemistry Experiment-Fourier-Transform Spectrometer (ACE-FTS) satellite data averaged over all longitudes and over the three most interesting latitude bands for stratospheric O_3: Antarctic (90–60°S), Tropics (30°S–30°N), and Arctic (60–90°N). In the upper stratosphere (3–10 hPa, see top row), the absolute value of the bias is generally less than $\pm 10\%$ for all instruments, except in 2003–2004 in the north polar region, where larger biases appear. This is related to the degraded quality of the assimilated SCIAMACHY and MIPAS data in 2003 and also to the lack of MLS O_3 profile data for assimilation until the beginning of August 2004 (Inness et al., 2019). A negative bias against MLS (maximum 4%), ACE-FTS (maximum 10%), and MIPAS (maximum 12%) is systematically present in this layer since mid-2004. All limb data sets show that this O_3 deficit has a seasonal component: The negative biases are more pronounced in summer than in

Table 2. Validation data sets. DOI: https://doi.org/10.1525/elementa.2020.00171.t2

Data set	Species	Vertical Range	Temporal Resolution	Validation Metrics	Uncertainties	References
Global Atmosphere Watch	CO, O_3	Surface	Hourly	Monthly MNMBs from 3-hourly comparisons	CO: ± 2 ppb for marine boundary layer sites and ± 5 ppb for continental sites. O_3: ± 1 ppb (WMO, 2013)	Eskes et al. (2015) and Wagner et al. (2015)
Ozone soundings from different networks	O_3	Stratosphere, free troposphere	Daily to weekly profiles	Monthly MNMBs from 3-hourly comparisons	Precision of 3%–5% (approximately 10% in the troposphere for Brewer Mast) and an accuracy of 5%–10% for the free troposphere and the stratosphere. Larger accuracies (up to 18%) may occur in altitudes above 28 km.	Deshler et al. (2008), Eskes et al. (2015), Smit et al. (2007, 2013), and Witte et al. (2018)
Network for the Detection of Atmospheric Composition Change	CO, O_3	Total column/ partial column	Multiple measurements per day	Monthly relative mean bias, correlation	CO: $\pm 4\%$, O_3: $\pm 3\%$	DeMazière et al. (2018)
European Monitoring and Evaluation Programme	O_3	Surface	Hourly	Monthly MNMBs from 3-hourly comparisons	± 1–2 ppb	Aas et al. (2001) and Torseth et al. (2012)
In-service Aircraft for a Global Observing System aircraft data	CO, O_3	Surface, troposphere, UTLS	Multiple measurements per day	Monthly MNMBs from daily comparisons	CO: ± 5 ppbv $+ 5\%$, O_3: ± 2 ppbv $+ 2\%$	Petzold et al. (2015) and Nédélec et al. (2015)
International Arctic Systems for Observing the Atmosphere	O_3	Surface	0.5–1 h	Monthly MNMBs from 3-hourly comparisons	O_3: ± 1 ppb (WMO, 2013)	https://www.esrl.noaa.gov/psd/iasoa/node/271. Accessed 4 May 2021.

O_3 = ozone; CO = carbon monoxide; MNMB = modified normalized mean bias; UTLS = upper troposphere lower stratosphere.

Table 3. Validation data sets for satellite data. DOI: https://doi.org/10.1525/elementa.2020.00171.t3

Satellite Data Set	Species	Vertical Range	Equatorial Overpass	Global Coverage	Spatial Resolution	Validation Metrics	Uncertainties	References
SCIAMACHY/ Envisat	NO$_2$, HCHO	Troposphere	10:00 LT	Approximately every 3 days	30 × 30 km^2 footprint gridded to approximately 0.75° × 0.75°	Monthly averages/ monthly MNMBs from 3-hourly comparisons	NO$_2$: approximately 20%–30% in polluted regions, HCHO: approximately 20%–40%	NO$_2$: Richter et al. (2005), HCHO: Wittrock et al. (2006)
GOME-2/ MetOp-A	NO$_2$, HCHO	Troposphere	9:30 LT	Near daily	2007–2013: 40 × 80 km^2 footprint/2013–present: 40 × 40 km^2 footprint gridded to approximately 0.75° × 0.75°	Monthly averages/ monthly MNMBs from 3-hourly comparisons	NO$_2$: approximately 20%–30% in polluted regions, HCHO: approximately 20%–40%	NO$_2$: Richter et al. (2011); HCHO: Vrekoussis et al. (2010)
ACE-FTS	O$_3$	Stratosphere	N/A	Global; up to 7,000 profiles/year; latitude distribution varying seasonally	N/A	Monthly NMBs from 6-hourly comparisons	Low and mid-strato: 5%; USLM: 20%	Sheese et al. (2017)
AURA MLS	O$_3$	Stratosphere	N/A	Approximately 3,500 profiles /day; latitude range −82° to +82°	N/A	Monthly NMBs from 6-hourly comparisons	Low and midstrato: 7%; USLM: 20%	Livesey et al. (2018)
MIPAS (ESA)	O$_3$	Stratosphere	N/A	Approximately 30,000 profiles/ month	N/A	Monthly NMBs from 6-hourly comparisons	Lower tropical strato: 10%–15%; other strato regions: 5%	Laeng et al. (2018)
Terra (MOPITT)	CO	Troposphere	10:30 LT	Approximately every 3 days	22 × 22 km^2 gridded to 1° × 1°	Monthly averages, MNMBs from 3-hourly comparisons	<10%	Deeter et al. (2017)
MetOp-A (IASI)	CO	Troposphere	9:30 LT	Near daily	12 km diameter footprint on the ground at nadir gridded to 1° × 1°	Monthly averages, MNMBs from 3-hourly comparisons	Approximately 10%; during, for example, fire events up to 17%	George et al. (2009)

O$_3$ = ozone; CO = carbon monoxide; NO$_2$ = nitrogen dioxide; HCHO = formaldehyde; LT = local time; MNMB = modified normalized mean bias; USLM = upper stratosphere/lower mesosphere; SCIAMACHY = Scanning Imaging Absorption Spectrometer for Atmospheric Chartography; GOME = Global Ozone Monitoring Experiment; ACE-FTS = Atmospheric Chemistry Experiment-Fourier-Transform Spectrometer; MIPAS = Michelson Interferometer for Passive Atmospheric Sounding; MOPITT = Measurements of Pollution in the Troposphere; IASI = Infrared Atmospheric Sounding Interferometer.

Table 4. Validation metrics. DOI: https://doi.org/10.1525/elementa.2020.00171.t4

Modified Normalized Mean Bias (MNMB)	Correlation Coefficient (R)	Fractional Error (FGE)	Gross	Root Mean Square Error (RMSE)	Mean Bias (MB)
$MNMB = \frac{2}{N}\sum_i \frac{f_i - o_i}{f_i + o_i}$	$R = \frac{\frac{1}{N}\sum_i (f_i - \bar{f})(o_i - \bar{o})}{\sigma_f \sigma_o}$	$Ef = \frac{2}{N}\sum_i \left| \frac{f_i - o_i}{f_i + o_i} \right|$		$RMSE = \sqrt{\frac{1}{N}\sum_i (f_i - o_i)^2}$	$B = \frac{1}{N}\sum_i (f_i - o_i)$

With $\bar{f}$ mean value of the reanalysis $\bar{o}$ mean observed value and σ_f, σ_o are the corresponding standard deviations.

Table 5. List of acronyms used in this article. DOI: https://doi.org/10.1525/elementa.2020.00171.t5

Acronym	Meaning
AC	Atmospheric composition
ACE-FTS	Atmospheric Chemistry Experiment-Fourier-Transform Spectrometer
ADS	Atmosphere Data Store
BL	Boundary layer
CAMS	Copernicus Atmosphere Monitoring Service
CB05	Carbon Bond 2005 chemical mechanism
CTM	Chemistry transport model
EMEP	European Monitoring and Evaluation Programme
FTIR	Fourier transform infrared
GAW	Global Atmosphere Watch
GFAS	Global Fire Assimilation System
GOME	Global Ozone Monitoring Experiment
HCHO	Formaldehyde
IAGOS	In-service Aircraft for a Global Observing System
IASOA	International Arctic Systems for Observing the Atmosphere
IASI	Infrared Atmospheric Sounding Interferometer
IFS	Integrated Forecasting System
IUP-UB	Institut für Umweltphysik Universität Bremen
LATMOS	Laboratoire Atmosphères, Observations Spatiales
LT	Local time
MACC	Monitoring Atmospheric Composition and Climate
MIPAS	Michelson Interferometer for Passive Atmospheric Sounding
MLS	Microwave Limb Sounder
MOPITT	Measurements of Pollution in the Troposphere
NCAR	National Center for Atmospheric Research
NDACC	Network for the Detection of Atmospheric Composition Change
NILU	Norwegian Institute for Air Research
NORS	Demonstration Network Of ground-based Remote-Sensing Observations
NRT	Near-real-time
RMS	Root mean square
SBUV	Solar Backscatter Ultraviolet Radiometer

(continued)

TABLE 5. *(continued)*

Acronym	Meaning
SCIAMACHY	Scanning Imaging Absorption Spectrometer for Atmospheric ChartographY
SH	Southern Hemisphere
SHADOZ	Southern Hemisphere Additional Ozonesondes
SL	Surface layer
TC	Total column
USLM	Upper stratosphere/lower mesosphere
UT	Upper troposphere
UTC	Coordinated universal time
UTLS	Upper troposphere lower stratosphere
UV	Ultraviolet
VOC	Volatile organic compound
WOUDC	World Ozone and Ultraviolet Radiation Data Centre
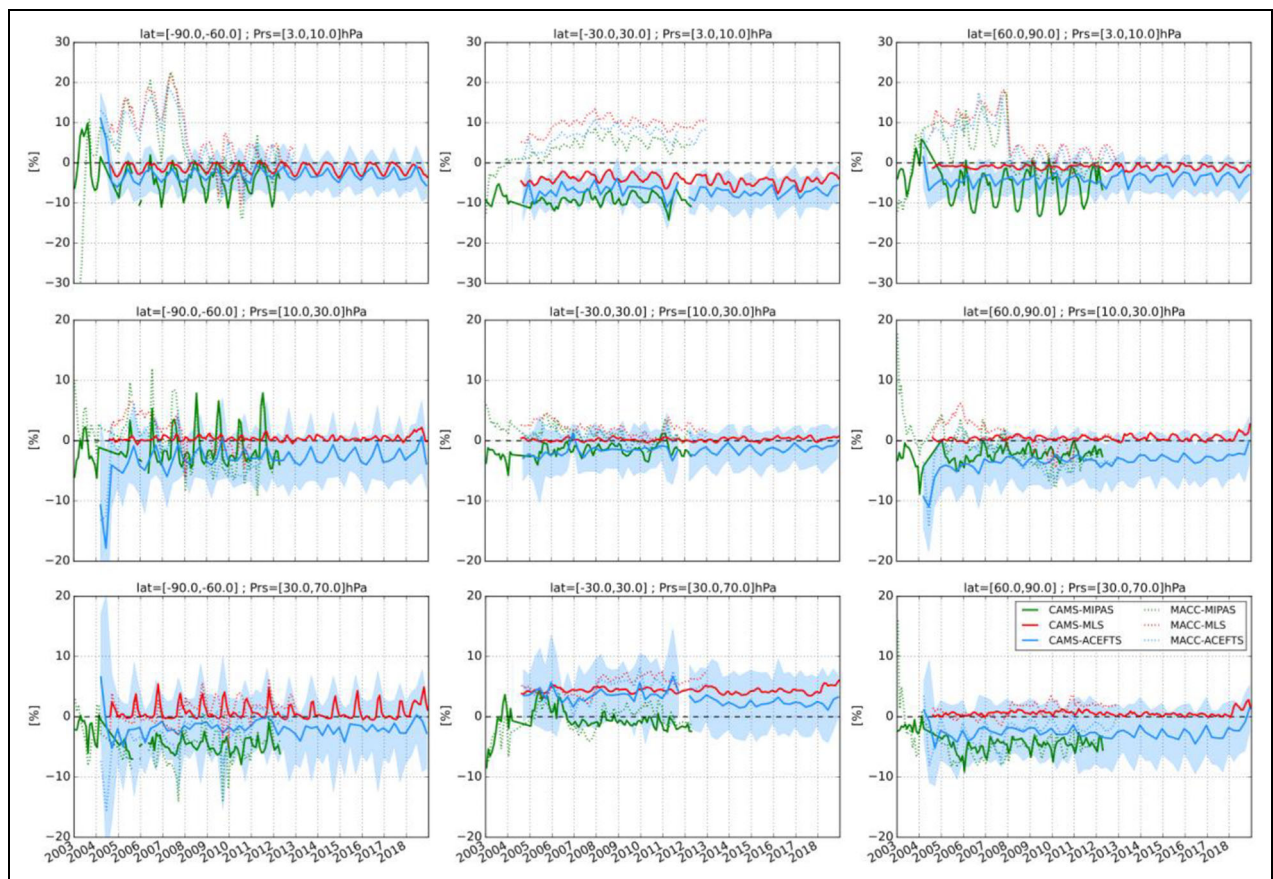
Figure 1. Modified normalized mean bias (MNMB, %) for the O_3 evaluation with satellite data. The time series compares the MNMB of O_3 of the CAMS reanalysis (solid lines) and MACC reanalysis (dotted lines) with observations from MIPAS (green), MLS (red), and ACE-FTS (blue) for the period January 1, 2003, to December 31, 2018, in the upper stratosphere (3–10 hPa mean, top row), middle stratosphere (10–30 hPa mean, middle row), and lower stratosphere (30–70 hPa mean, bottom row) for three latitude bands, respectively: South Pole (90–60°S, left column), Tropics (30°S–30°N, central column), and North Pole (60–90°N, right column). The envelope around the bias between CAMS reanalysis and ACE-FTS represents two normalized standard deviations of the differences. O_3 = ozone; CAMS = Copernicus Atmosphere Monitoring Service; MACC = Monitoring Atmospheric Composition and Climate; MIPAS = Michelson Interferometer for Passive Atmospheric Sounding; MLS = Microwave Limb Sounder; ACE-FTS = Atmospheric Chemistry Experiment-Fourier-Transform Spectrometer. DOI: https://doi.org/10.1525/elementa.2020.00171.f1
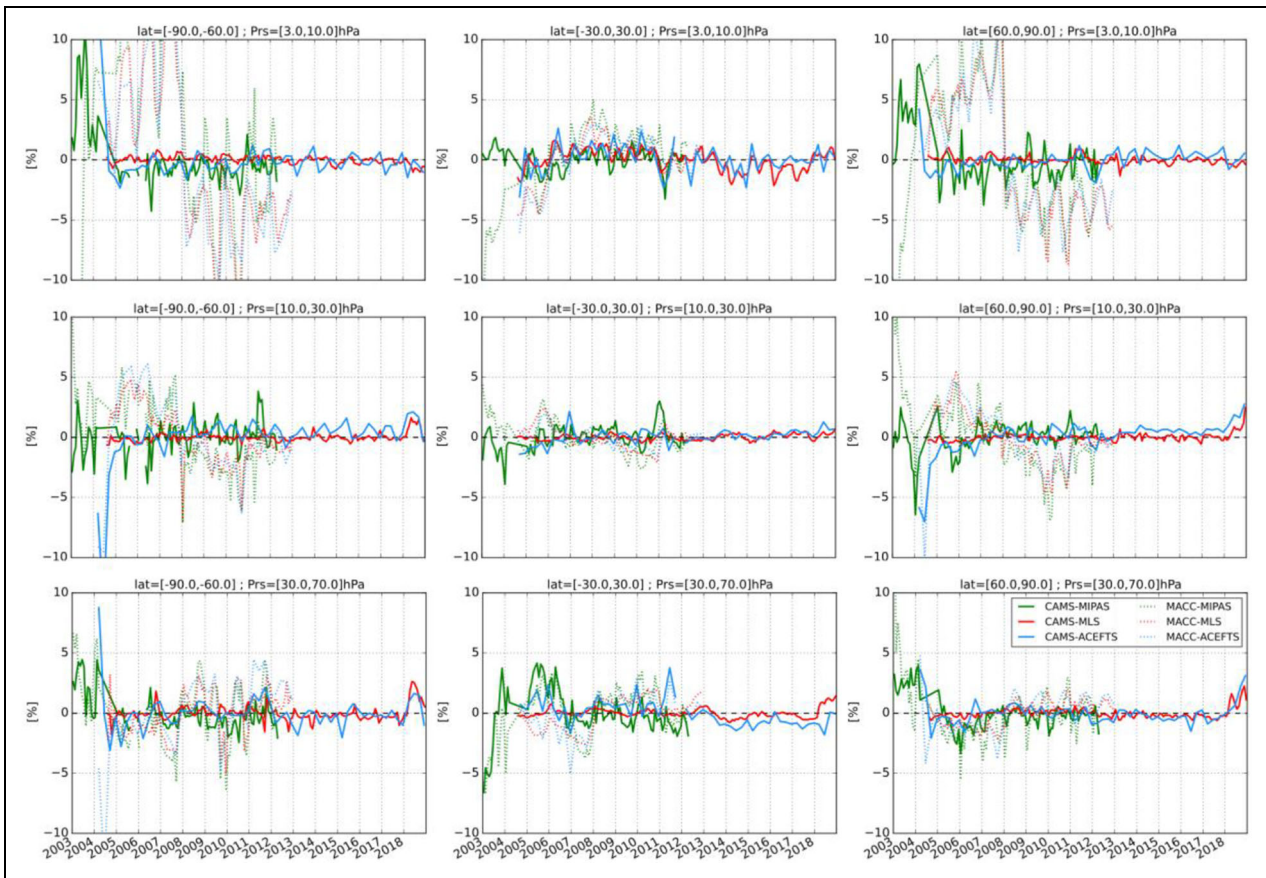
Figure 2. Deseasonalized time series of the MNMB (%) shown in **Figure 1**. The deseasonalization is done by the removal of the corresponding monthly climatologies shown in Figure S2. MNMB = modified normalized mean bias. DOI: https://doi.org/10.1525/elementa.2020.00171.f2

winter (see Figure S2). The seasonal biases with respect to MLS are much smaller than for MIPAS. This indicates that the CAMS reanalysis is much more constrained by MLS than by MIPAS and that the seasonal patterns mostly reflect differences between MIPAS and MLS. Seasonal biases between MIPAS and MLS have already been published for the midlatitudes (Errera et al., 2019) and are shown here in the tropical and polar regions. While such interinstrument biases deserve more investigation, they are beyond the scope of this article.

In the middle stratosphere (10–30 hPa, middle row), after 2004, the bias is generally within $\pm 5\%$ for all limb-scanning satellite data sets. This is in very good agreement with a recent comparison of ACE-FTS with MLS and MIPAS observations, which also reports biases within 5% in the middle stratosphere (Sheese et al., 2017). In the lower stratosphere (30–70 hPa, bottom row), the spread of the biases against the different instruments is larger. The bias against MLS and ACE-FTS is positive (3%–7%) in the Tropics. In the polar regions, the bias against MLS is low (<1.5%), except during the O_3 hole events (September–October in the $90°–60°$S latitude band) when O_3 abundances are approximately 3% larger than in the MLS data set, that is, O_3 depletion is slightly underestimated. The biases against MIPAS and ACE-FTS are negative but remain always lower than 10% and 5%, respectively.

Figure 2 presents the deseasonalized time series of the normalized mean biases based on the monthly climatologies shown in Figure S2. The importance of high-quality assimilation data most obviously shows for the year 2003, where the limited availability of such data has a negative impact on the validation results. The bias against ACE-FTS is stable over time, except for a slight drift after 2013 in the lower tropical stratosphere (but <1% over 5 years). The deseasonalized biases with both MLS and ACE-FTS exhibit an increase of approximately 2% over the last year (2018) in the polar middle stratosphere and in all three regions of the lower stratosphere. This feature continues in 2019 and is likely related to the switch from reprocessed to NRT MLS V4 data.

Figure S3 gives a global overview of the agreement between the CAMS and MACC reanalysis and the observations by the limb-scanning instruments, averaged over the whole period. The correlation between the reanalysis and the observations is very good (at least >0.8 for the pressure range 2–200 hPa or altitude range 10–45 km for ACE-FTS).

The CAMS reanalysis setup does not include explicit modeling of stratospheric chemistry. The stratospheric O_3 profile is constrained using the Cariolle parametrization (e.g., Cariolle and Teyssèdre, 2007). In practice, this leads to considerable biases in the stratospheric profile observed in the control run when comparing with
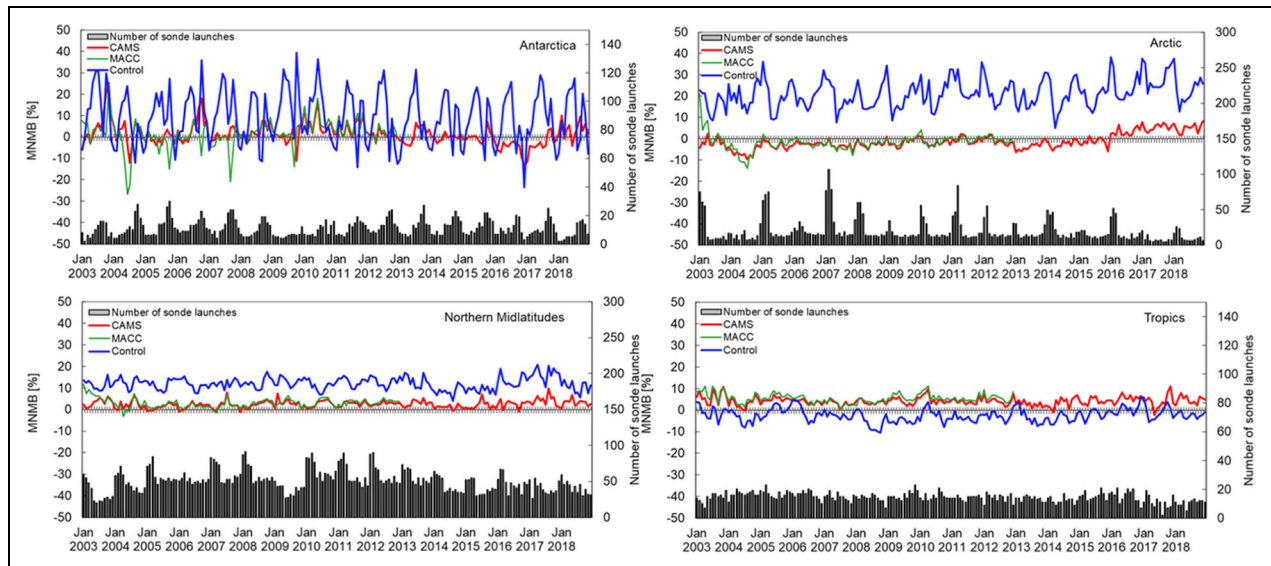
Figure 3. Time series of monthly modified normalized mean biases against ozonesondes for the stratosphere between 2003 and 2018. Top left: Antarctica, top right: the Arctic, bottom left: Northern midlatitudes, bottom right: Tropics (red: CAMS reanalysis, blue: Control run, green: MACC reanalysis). The profiles are averaged between 90 and 10 hPa in the extra-tropics and between 60 and 10 hPa in the Tropics. CAMS = Copernicus Atmosphere Monitoring Service; MACC = Monitoring Atmospheric Composition and Climate. DOI: https://doi.org/10.1525/elementa.2020.00171.f3

O_3sonde (**Figure 3**; Figures S4–S7, Table S2) and NDACC data (Figure S8, Table S3) in the stratosphere, reflecting uncertainties in the Cariolle O_3 parametrization. Large positive biases of up to 40% appear over Antarctica and the Arctic and modified normalized mean biases (MNMBs) up to 20% over the Northern midlatitudes. For NDACC stations in the Southern midlatitudes and over the Tropics, the control run shows negative biases up to −15% (Figure S8).

The assimilation of O_3 total columns and stratospheric profiles in the CAMS reanalysis successfully compensates for this lack in explicit stratospheric chemistry and thus proves to be very effective in constraining stratospheric O_3. The seasonal and interannual evaluation with O_3sonde data shows a very stable and consistent performance of the CAMS reanalysis during all years and seasons (Figures S4–S7) with MNMBs mostly smaller than 5%. Only over the Arctic, a very small change in bias from negative to positive is visible from 2017 onward, which likewise appears in the control run.

3.2. Tropospheric ozone
In the troposphere, our validations rely on sonde observations (**Figure 4**; Table S4) and In-service Aircraft for a Global Observing System (IAGOS) measurements (**Figure 5**; Table S5).

For the CAMS reanalysis, MNMBs in all regions are mostly within 10%, with respect to sonde observations. Larger positive biases appear over the Tropics and Antarctica.

The control run underestimates O_3 with MNMBs between 10% and 20% in all regions except the Tropics, where O_3 is overestimated with MNMBs up to 20% (**Figure 4**; Figures S9–S11). The continual overestimation of O_3 could potentially relate to an overestimation of

precursor emissions (fire and biogenic emissions) in this region (see Section 3.4). In the high latitudes and Northern midlatitudes, the control run has a seasonal pattern in the bias, with larger negative biases during winter and spring.

Data assimilation effectively increases tropospheric O_3, which improves MNMBs in most regions for the CAMS reanalysis compared to the control run. Likewise, the seasonality in the biases is largely eliminated by the data assimilation. In the Tropics, data assimilation is less effective in improving the biases for the CAMS reanalysis compared to the control run.

Two periods with larger MNMBs in the time series are noticeable for the CAMS reanalysis, which affect the long-term consistency and relate to data assimilation issues: Firstly, from 2003 to 2004, where MNMBs show a drop until August 2004 (**Figure 4**), already explained in the stratospheric section. Secondly, from 2013 onward, where MNMBs of the CAMS reanalysis are suddenly increasing especially over Antarctica. The change in MNMBs is accompanied by a more pronounced seasonal variation of biases. The interannual seasonal time series in **Figure 6** and Figures S9–S11 clearly shows shifts in MNMB, which are most distinct over the high latitudes (Arctic, Antarctica). This effect was still under investigation in the study of Inness et al. (2019). It can now be attributed to the switch from 13 L V8.6 SBUV/2 to 21 L NRT SBUV/2 data in July 2013 and might also be affected by the loss of Envisat data in April 2012 (SBUV: Solar Backscatter Ultraviolet Radiometer). These changes in the assimilation system cause a jump in the bias in December to February (DJF) over Antarctica and a drop in biases in June to August (JJA; **Figure 6**). Over the Arctic and Northern midlatitudes, biases likewise drop during DJF 2013/2014 (Figures S9 and S10). In the
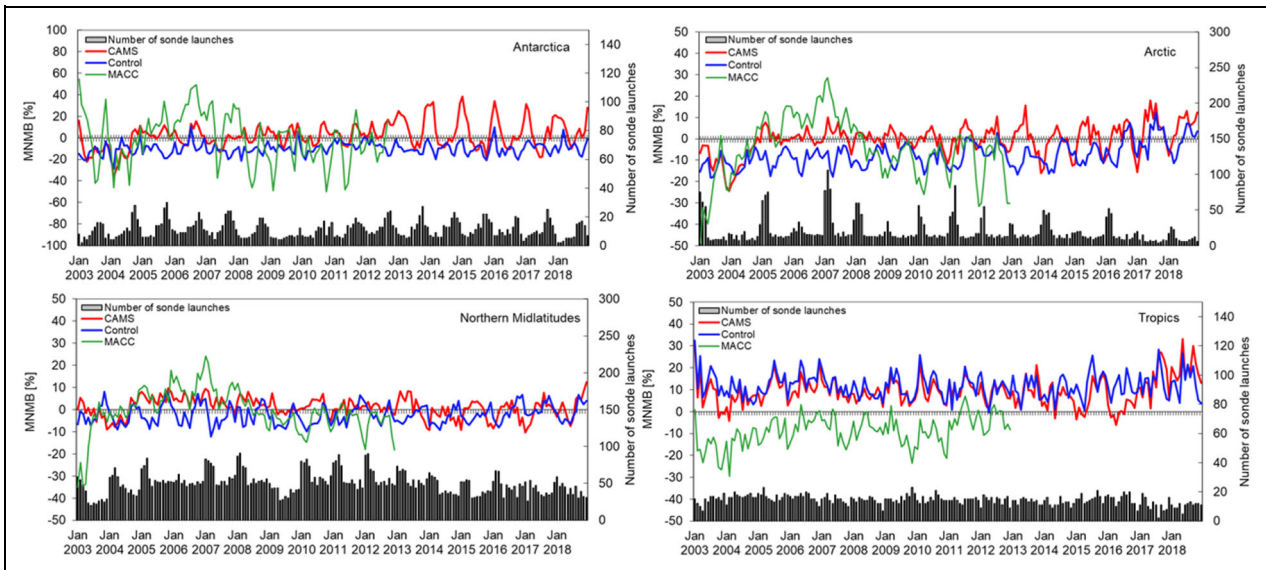
Figure 4. Time series of monthly MNMBs (%) from the validation with ozonesondes for the free troposphere between 2003 and 2018. Top left: Antarctica, top right: Arctic, bottom left: Northern midlatitudes, bottom right: Tropics (red: CAMS reanalysis, blue: control run, green: MACC reanalysis). The plots show an average over the altitude range between 750 and 200 hPa in the Tropics and between 750 and 350 hPa elsewhere. MNMBs = modified normalized mean biases; CAMS = Copernicus Atmosphere Monitoring Service; MACC = Monitoring Atmospheric Composition and Climate. DOI: https://doi.org/10.1525/elementa.2020.00171.f4
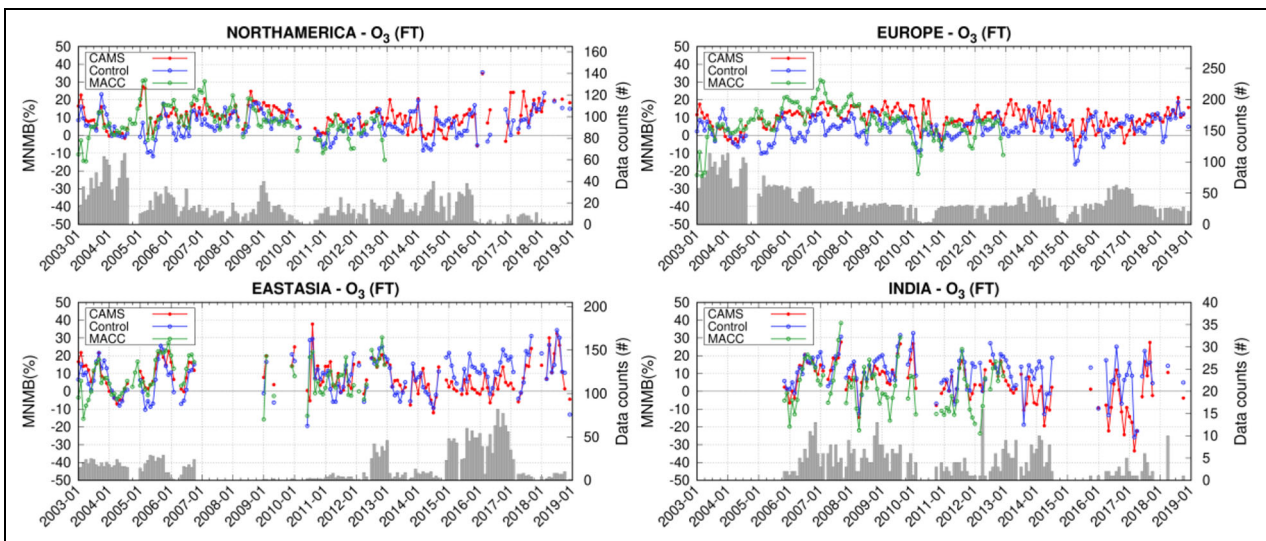
Figure 5. Time series of monthly MNMBs (%) from the comparison against In-service Aircraft for a Global Observing System O_3 aircraft data in the free troposphere for the period 2003–2018. Top left: North America, top right: Europe, bottom left: East Asia, bottom right: India. The plots show averages over various airports in the free troposphere (350–850 hPa) for the CAMS reanalysis (red), control run (blue), and MACC reanalysis (green). MNMBs = modified normalized mean biases; CAMS = Copernicus Atmosphere Monitoring Service; MACC = Monitoring Atmospheric Composition and Climate; O_3 = ozone . DOI: https://doi.org/10.1525/elementa.2020.00171.f5

Tropics, we find larger differences between the control run and the CAMS reanalysis after these changes in 2013 (Figure S11).

The evaluation with IAGOS data shows MNMBs of −5% and 25% over North America, −10% to 20% over Europe, between −10% and 40% over East Asia, and ±35% over India (**Figure 5**). O_3 is mostly overestimated over the more polluted metropolitan sites, especially over India and East Asia (see Figures S12–S15). The control run has larger positive MNMBs over India and partly over East Asia, but lower MNMBs over Europe and North America (see also Figure S16). Over India and East Asia, biases increase during July–September, revealing problems of the model to correctly simulate the low O_3 values during the Asian monsoon season (Figure S16). The seasonal pattern in the biases is almost absent for
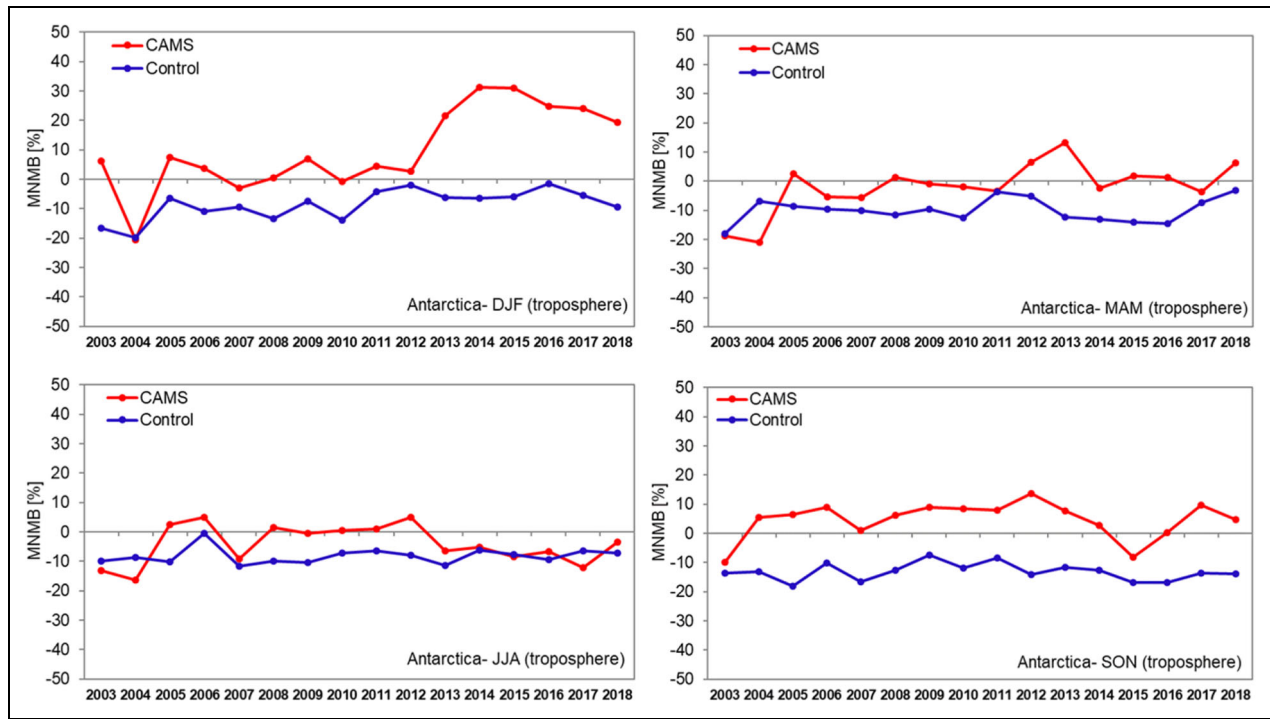
Figure 6. Interannual time series of seasonal MNMBs (%) from the validation with ozonesondes in the free troposphere for Antarctica between 2003 and 2018. Top left: DJF, top right: MAM, bottom left: JJA, bottom right: SON (CAMS reanalysis: red, control run: blue). MNMBs = modified normalized mean biases; CAMS = Copernicus Atmosphere Monitoring Service; DJF = December to February; MAM = March to May; JJA = June to August; SON = September to November. DOI: https://doi.org/10.1525/elementa.2020.00171.f6
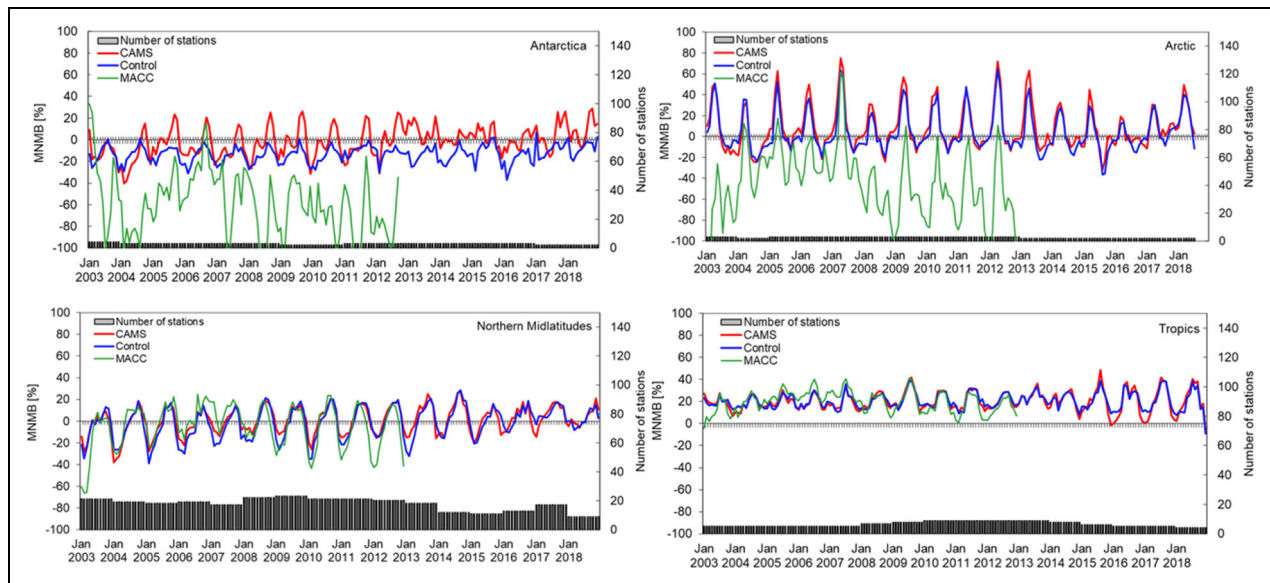

Figure 7. Time series of monthly MNMBs (%) from the comparison against surface O_3 from Global Atmosphere Watch stations between 2003 and 2018. Top left: Antarctica, top right: Arctic, bottom left: Northern midlatitudes, bottom right: Tropics (red: CAMS reanalysis, blue: Control run, green: MACC reanalysis). MNMB = modified normalized mean biases; CAMS = Copernicus Atmosphere Monitoring Service; MACC = Monitoring Atmospheric Composition and Climate; O_3 = ozone. DOI: https://doi.org/10.1525/elementa.2020.00171.f7

Europe and North America and reduced for India and East Asia for the CAMS reanalysis, which is more constant over the years, however, with partly larger positive biases compared to the control run.

3.3. Surface ozone

Modeled surface O_3 is compared to Global Atmosphere Watch (GAW) data (**Figure 7**), International Arctic Systems for Observing the Atmosphere (IASOA) network
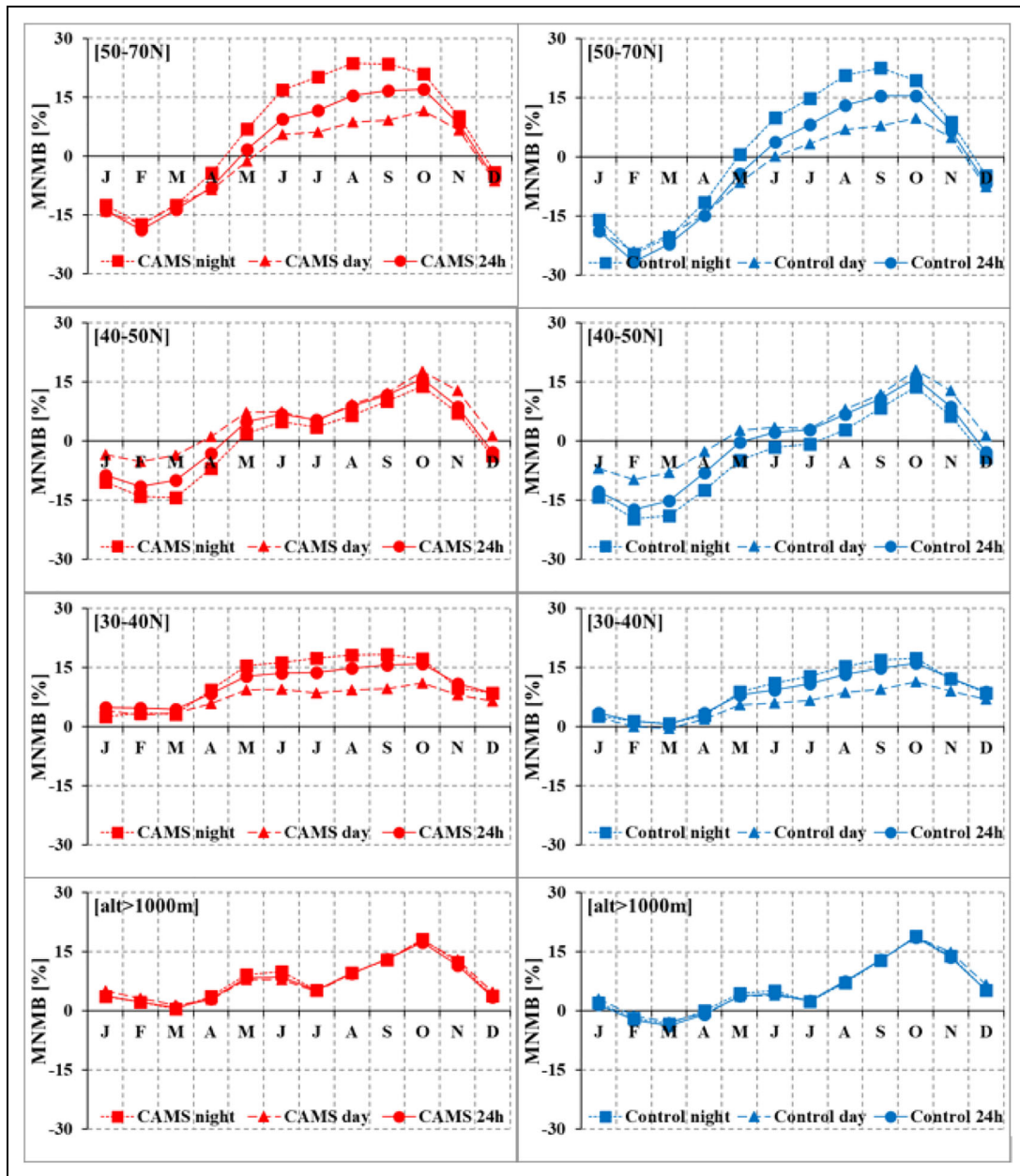
Figure 8. Mean O_3 seasonal variability of MNMBs for the period 2003–2018 from the comparison with European Monitoring and Evaluation Programme surface data. For nighttime (0–3 UTC, squares), for daytime (12–15 UTC, triangles), and for the whole 24 h (circles), over Northern Europe (1st row), Central Europe (2nd row), Southern Europe (3rd row), as well as for stations with an altitude greater than 1,000 m above sea level (4rd row; CAMS reanalysis: red on the left, control run: blue on the right). MNMBs = modified normalized mean biases; CAMS = Copernicus Atmosphere Monitoring Service; UTC = coordinated universal time; O_3 = ozone. DOI: https://doi.org/10.1525/elementa.2020.00171.f8

data (Figure S17), European Monitoring and Evaluation Programme (EMEP) observations (**Figure 8** and Figure S18) and to IAGOS aircraft measurements (Figure S19).

Figure 7 shows the time series of MNMBs for surface O_3 calculated from model and GAW observational data, as regional average over stations in four different latitude zones. Biases for surface O_3 are generally larger than for O_3 in the free troposphere but remain within $\pm 30\%$. Largest biases for both CAMS reanalysis and control run appear during Arctic spring (MNMBs up to 80%).

A closer look at Arctic stations from the IASOA network (Figure S17, Table S6) reveals that the High Arctic coastal stations (Alert, Barrow, and Villum Research Station) are influenced by O_3 depletion events during arctic spring (MAM: March to May). These halogen chemistry reactions are not represented in the simulations, and the model is thus unable to capture the low concentrations measured in spring at these sites. European Arctic IASOA sites (Esrange, Karasjok, Oulanka, Pallas, and Tustervatn), which are located inland, are not affected by O_3 depletion events and thus show smaller biases during springtime (see Figure S17).
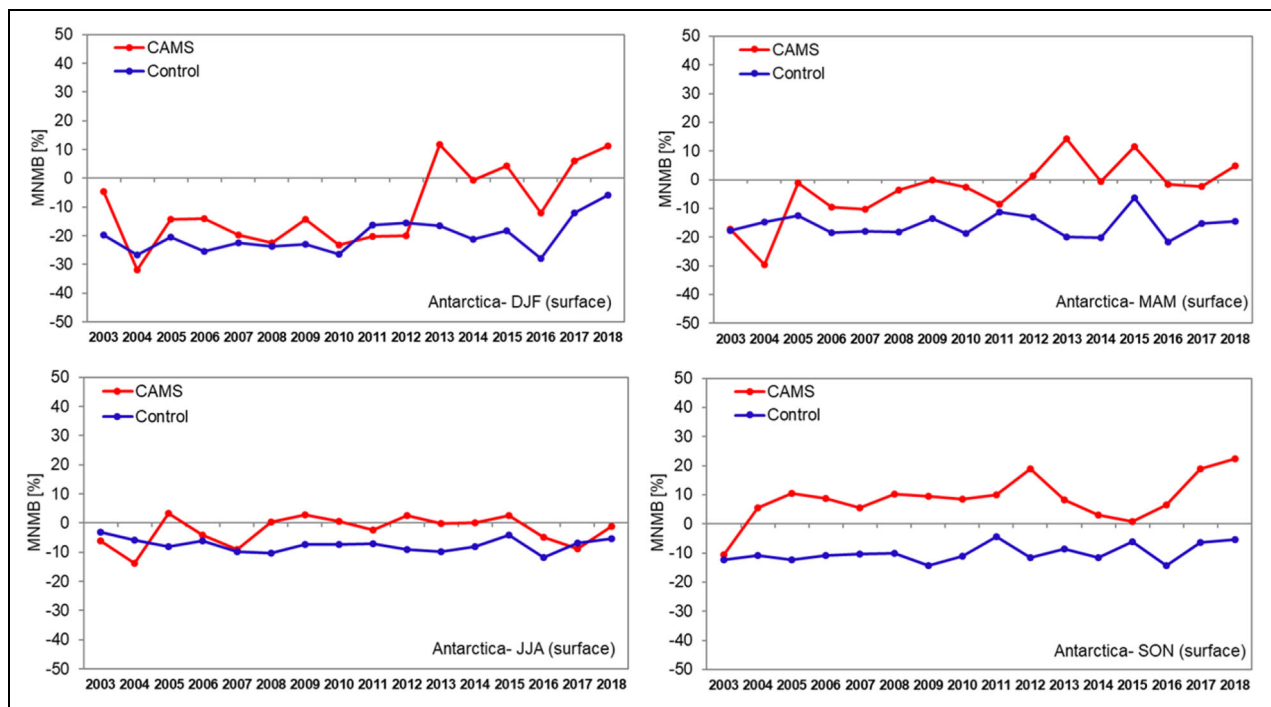
Figure 9. Interannual time series of seasonal MNMBs (%) from the validation with Global Atmosphere Watch surface data for Antarctica between 2003 and 2018. Top left: DJF, top right: MAM, bottom left: JJA, bottom right: SON (CAMS reanalysis: red, Control run: blue). MNMBs = modified normalized mean biases; CAMS = Copernicus Atmosphere Monitoring Service; DJF = December to February; MAM = March to May; JJA = June to August; SON = September to November. DOI: https://doi.org/10.1525/elementa.2020.00171.f9

Our evaluations show that the impact of data assimilation is rather small at the surface, which reflects in almost identical biases for the CAMS reanalysis and control run (**Figure 7**; Figures S17–S19). Differences between the control run and the CAMS reanalysis appear for high-latitude regions (**Figure 9**; Figure S20), where data assimilation increases surface O_3, which partly improves the negative bias in the control run but partly also leads to overestimations of modeled O_3, especially during Arctic/Antarctic spring (MAM/SON, respectively; SON = September to November).

For Antarctica (**Figure 9**), the changes in the assimilation system described for tropospheric O_3 are visible even at the surface in a distinct shift in bias from negative to positive during DJF, and MAM 2012/2013, whereas the control run remains stable.

In the Northern midlatitudes (**Figure 7**), the interannual time series of biases show a constant seasonal pattern in the biases, with negative biases during DJF and MAM and larger positive biases during JJA and SON. This seasonal pattern in surface O_3 biases is very common in global CTMs and has been discussed in various studies before (e.g., Ordóñez et al., 2010; Val Martin et al., 2014; Wagner et al., 2015).

For Europe, we have additionally investigated these seasonal variations of MNMBs for different latitude zones for EMEP data sets (**Figure 8**). The seasonal mean variability of biases for the CAMS reanalysis has been separated in nighttime (0–3 UTC) and in midday time (12–15 UTC) values (UTC: coordinated universal time). For Northern

Europe, and to a smaller extent for Southern Europe, the overestimation in summer and underestimation during winter are stronger for nighttime O_3 than for daytime O_3. This likely means that nocturnal O_3 destruction processes in the boundary layer (like NO_x titration) are not reproduced correctly in the model. The global model has difficulties to resolve such regional subgrid processes (see e.g., Wagner et al., 2015). For stations above 1,000 m, only positive biases are present throughout the year without changes between nighttime and daytime. The overestimation reaches a maximum in October (MNMBs of 15%).

There is a drift in the interannual time series of seasonal MNMBs toward larger positive biases for the Northern midlatitudes (**Figure 10**). Similar drifts can be observed in the evaluation with EMEP data for Northern Europe (Figure S18) as well as in the evaluation with IAGOS surface data over Europe and East Asia (Figures S19 and S21). Park et al. (2020) accordingly note inadequateness of the CAMS reanalysis to capture O_3 trends for East Asia. In the Tropics, a drift is visible for JJA (Figure S22).

Although further investigations and sensitivity analysis will be needed to prove this, it is likely that unreasonable trends in the emissions are responsible for the drifts (see Section 3.4). In a recent study, Gaubert et al. (2020) show that running CTMs with biased CO and volatile organic compound (VOC) emissions can lead to poorly modeled O_3.

Compared to the previous MACC reanalysis, we see large improvements for the CAMS reanalysis for O_3 (see
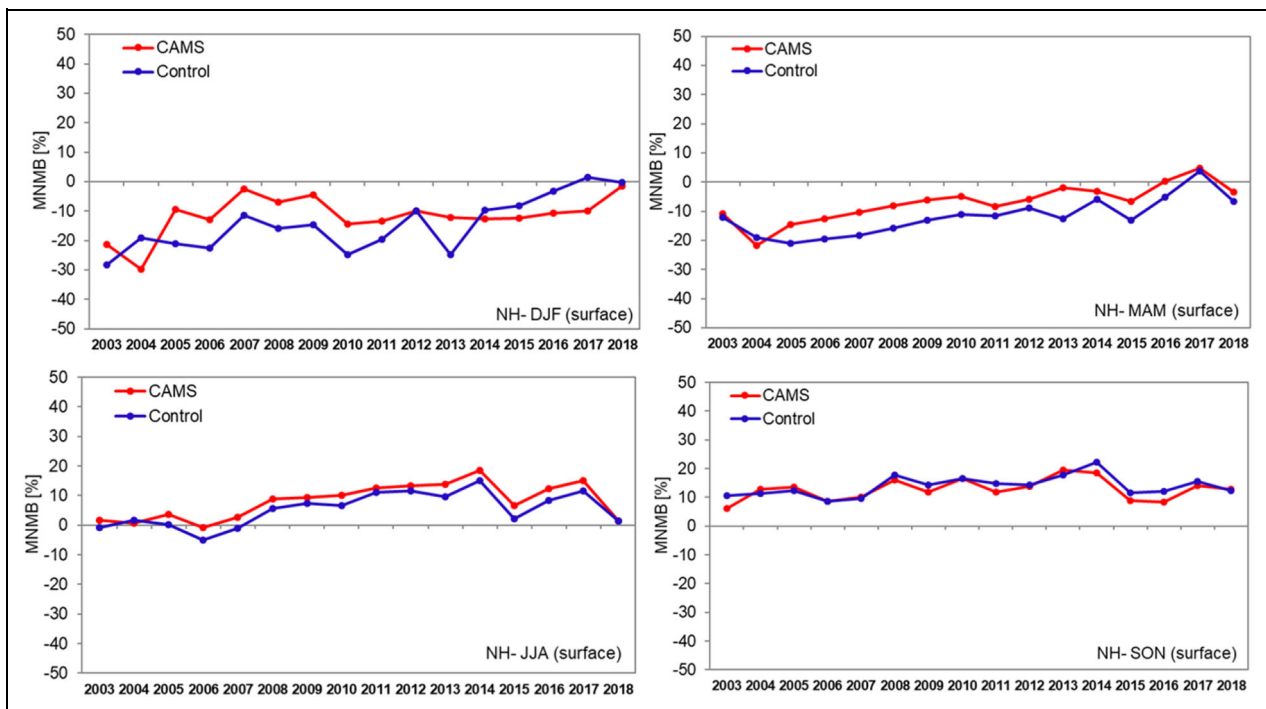
Figure 10. Interannual time series of seasonal MNMBs (%) from the validation with Global Atmosphere Watch surface data for the Northern midlatitudes between 2003 and 2018. Top left: DJF, top right: MAM, bottom left: JJA, bottom right: SON (CAMS reanalysis: red, control run: blue). MNMBs = modified normalized mean biases; CAMS = Copernicus Atmosphere Monitoring Service; DJF = December to February; MAM = March to May; JJA = June to August; SON = September to November. DOI: https://doi.org/10.1525/elementa.2020.00171.f10

Figures 1–5 and **Figure 7**; Tables S3, S7, and S8): in the upper and middle stratosphere over the poles, the refinements compared to the MACC reanalysis are most striking. The overestimation of O_3 below around 15 hPa completely disappears in the CAMS reanalysis due to a better setup of the variational bias correction scheme, which is now applied only to total column O_3 retrievals but not to profiles from MLS or MIPAS (Inness et al., 2013, 2019). The absence of the drift also leads to improvements for the free troposphere and surface. Apart from the drift, the MACC reanalysis also shows large negative biases (MNMBs down to –150%) in the high latitudes (**Figure 7**). This is a known issue of the former coupled IFS-MOZART-3 (MOZART: Model for OZone And Related chemical Tracers) CTM used in MACC (see e.g., Wagner et al., 2015). The improvements from MACC to CAMS mostly relate to changes in the chemistry module, that is, the replacement of the coupled model system (IFS and MOZART-3 CTM) used for the MACC reanalysis by the online-coupled model C-IFS (with CB05 of the TM5 CTM) used for the CAMS reanalysis (Flemming et al., 2015). As a result, MNMBs, especially in high-latitude regions, are considerably smaller and more stable. Furthermore, the seasonality of O_3 is better captured.

3.4. Carbon monoxide

Modeled CO is compared to Measurements of Pollution in the Troposphere (MOPITT) and Infrared Atmospheric Sounding Interferometer (IASI) total column satellite measurements (**Figures 11** and **12**; Figures S23 and S24), to

NDACC partial column measurements (**Figure 13**; Figure S25 and Table S9), and to IAGOS aircraft data (**Figure 14**; Figures S26 and S27 and Tables S10 and S11) and GAW CO surface observations (**Figure 15**; Figures S28 and S29 and Table S12).

Figure 11 shows MOPITT total column values as a function of latitude and time and the biases in comparison with the CAMS reanalysis and control. Observed CO total columns are slightly underestimated by the model over all regions with MNMBs mostly within ±10%. Larger MNMBs (up to 20%) appear over tropical regions, especially during the years 2012–2015.

The control run has larger CO in all regions, especially during the winter season. Largest positive MNMBs (up to 50%) show up over the Southern Hemisphere (SH) during November to May. For later years (2012 onward), the overestimation also reaches over to the northern hemispheric low latitudes. This effect in the control run accordingly appears in the validation with NDACC data in the SH (**Figure 13**) and has likewise been described by Flemming et al. (2017) for the CAMS interim reanalysis. In their study, the authors assume that the overestimation of CO in the SH points to deficiencies in the simulation of the global chemical loss and production of CO as well as problems with large-scale transport. To a minor extent, an overestimation of the GFAS biomass burning emissions for Central Africa, Maritime South East Asia, and South America could also seasonally contribute to this according to Flemming et al. (2017). In the frame of our validations, we find that the biogenic VOC emissions (MEGAN-MACC;
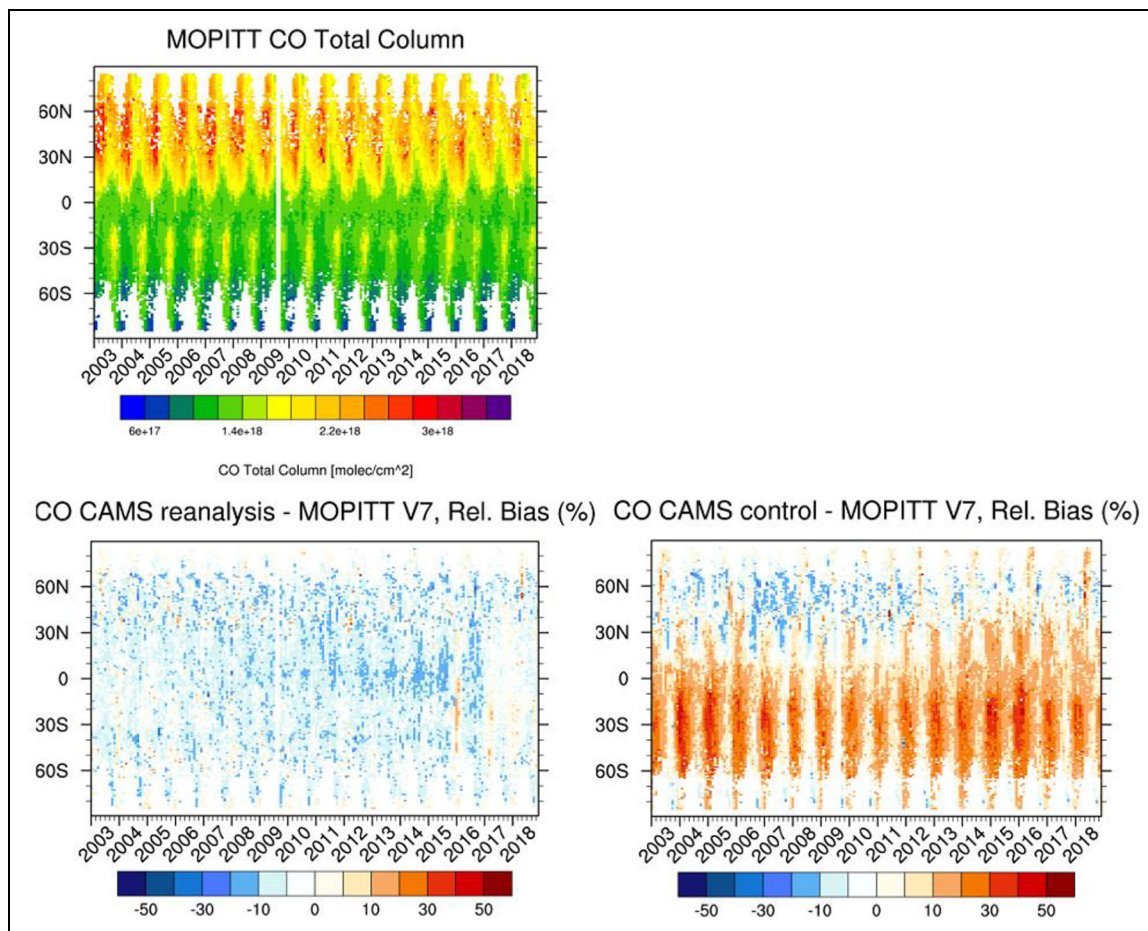
Figure 11. Measurements of Pollution in the Troposphere (MOPITT) V7 CO total column (upper panel) as a function of latitude and time from January 2003 to December 2018. Relative biases between MOPITT V7 and the CAMS reanalysis (lower panel, left) and between MOPITT V7 and the control run (lower panel, right). CAMS = Copernicus Atmosphere Monitoring Service; CO = carbon monoxide. DOI: https://doi.org/10.1525/elementa.2020.00171.f11

Sindelarova et al., 2014; Sindelarova, 2018) as chemical source term for CO may also play a considerable role concerning the overestimation of CO in the SH observed for the control run, as discussed below. In a comparison of available isoprene emission data, Sindelarova (2018) shows that the MEGAN-MERRA biogenic emissions (used in the CAMS reanalysis and control run) are about 1.5–2 times higher and show larger year-to-year differences than other available data sets. Additionally, the TM5 model seems to be more sensitive to changes in VOC (NMVOC) rates, as described by Zeng et al. (2015). In combination with larger biogenic emissions, this effect might contribute to the variation and magnitude of biases for CO shown for the control run. Data assimilation reduces total column CO for the CAMS reanalysis compared to the control run, and positive biases remain only for stations in the high latitudes of the SH (see **Figure 13**).

Figure S23 displays observed time series of total column CO concentrations of MOPITT and IASI in comparison to the CAMS reanalysis and control run over different regions. **Figures 12** and S24 show the resulting time series of MNMBs. The differences of total column CO between MOPITT and IASI are discussed by, for example, Illingworth et al. (2011) and George et al. (2015) and will

not be further addressed in the frame of this article. For Europe and the United States, biases of the CAMS reanalysis compared with total column data remain stable over the entire period with a seasonal variation showing larger underestimation during the summer season (up to -12%) and lower underestimation during winter (up to -5%). A similar seasonal pattern appears over East Asia and South Africa, whereas over North Africa, it is reversed. For IASI data, the seasonal pattern is stronger, and MNMBs are generally larger (up to -18% in summer and $\pm 8\%$ in winter). The control run, however, has larger variable CO concentrations over all regions. In comparison with MOPITT, this partly leads to an overestimation of CO during the winter season (Europe, United States, and East Asia).

The variability in the time series of biases in the control run closely resembles the annual variability of the CO burden of the control run, with low total column CO in 2008 (a La Niña year) and large total column CO in 2015 (an El Niño year with high fire activity). Main drivers for the spatial and temporal CO burden are wildfire emissions and anthropogenic emissions (Flemming and Inness, 2019).

An overestimation of fire emissions could explain larger CO in the SH and maxima during the El Niño year
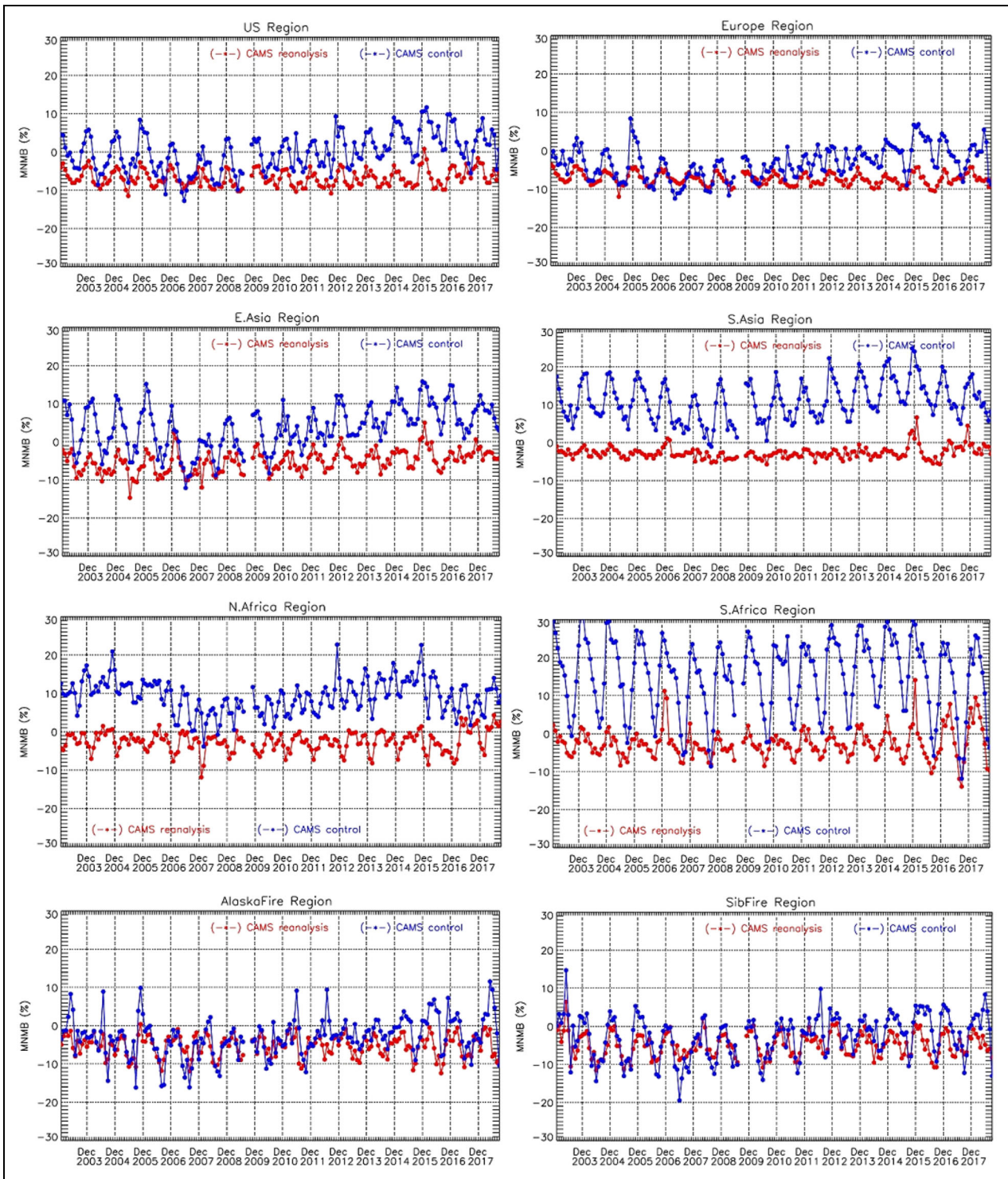
Figure 12. Time series of MNMBs bias (%) from the validation with Measurements of Pollution in the Troposphere v7 CO total columns over selected regions for the years from 2003 to 2018. First row left: the United States, first row right: Europe, second row left: East Asia, second row right: South Asia, third row left: North Africa, third row right: South Africa, last row left: Alaska fire region, last row left: Siberian fire region (CAMS reanalysis: red; control run: blue). MNMBs = modified normalized mean biases; CAMS = Copernicus Atmosphere Monitoring Service; CO = carbon monoxide. DOI: https://doi.org/10.1525/elementa.2020.00171.f12

2015. However, it does not explain the variability observed for other years like the increasing biases between 2011 and 2015 in the control run.

Various studies (Hassler et al., 2016; Elguindi et al., 2020) describe an inaccurate representation of CO emission trends in the MACCity inventory for Europe and the United States. Hassler et al. (2016) show that reduction trends of vehicle CO emissions in U.S. cities after 2007 are not captured correctly in the MACCity inventory. Elguindi et al. (2020) show large uncertainties for regions like
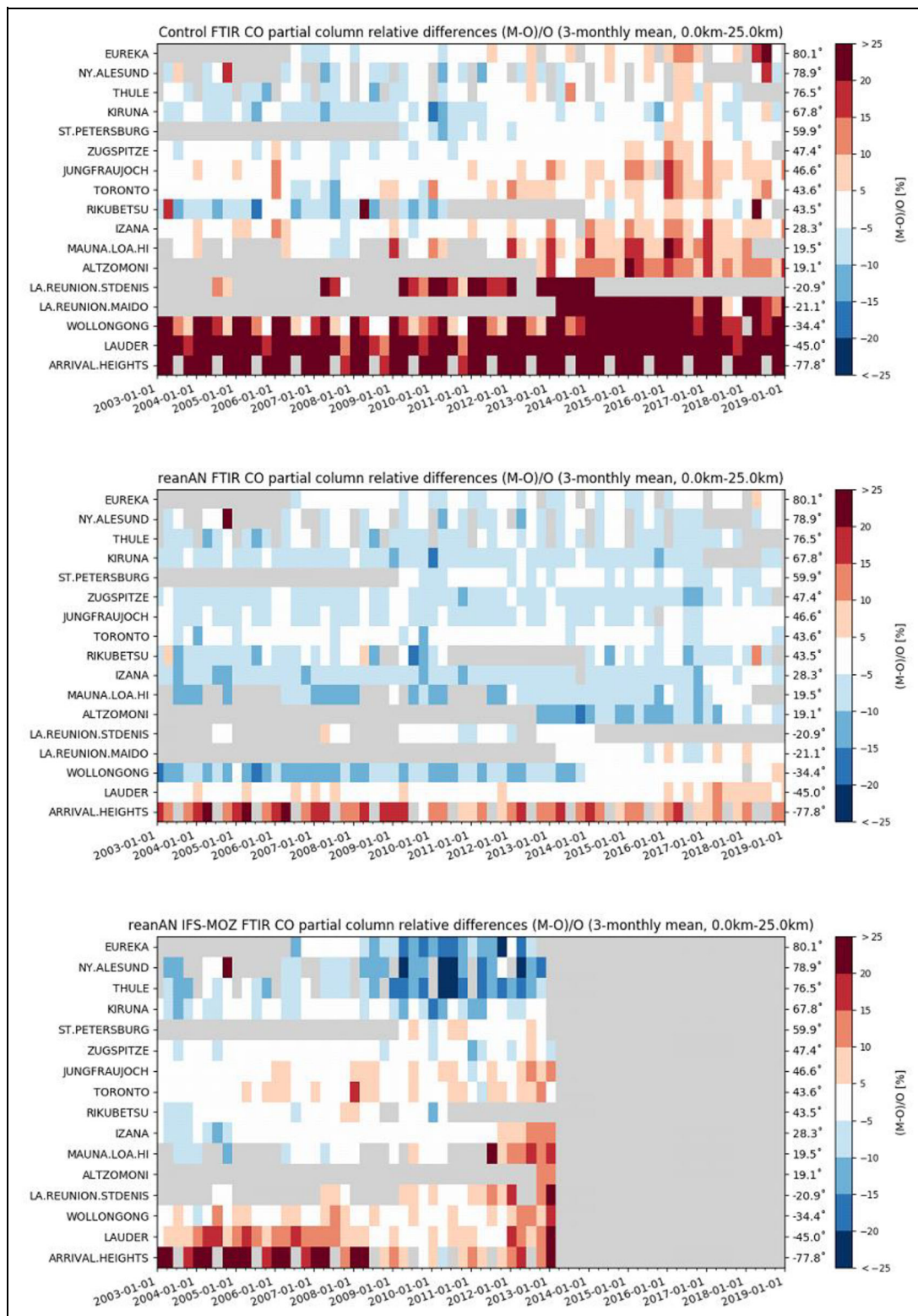
Figure 13. Time series of seasonal bias (DJF, MAM, JJA, and SON) for each Network for the Detection of Atmospheric Composition Change Fourier-transform infrared site. Top is CAMS control run, middle is CAMS reanalysis, and bottom is MACC reanalysis—sorted by decreasing latitude for the time period 2003–2018. The plot shows relative differences of the models compared to CO Fourier-transform infrared partial columns. CAMS = Copernicus Atmosphere Monitoring Service; MACC = Monitoring Atmospheric Composition and Climate; DJF = December to February; MAM = March to May; JJA = June to August; SON = September to November; CO = carbon monoxide. DOI: https://doi.org/10.1525/elementa.2020.00171.f13
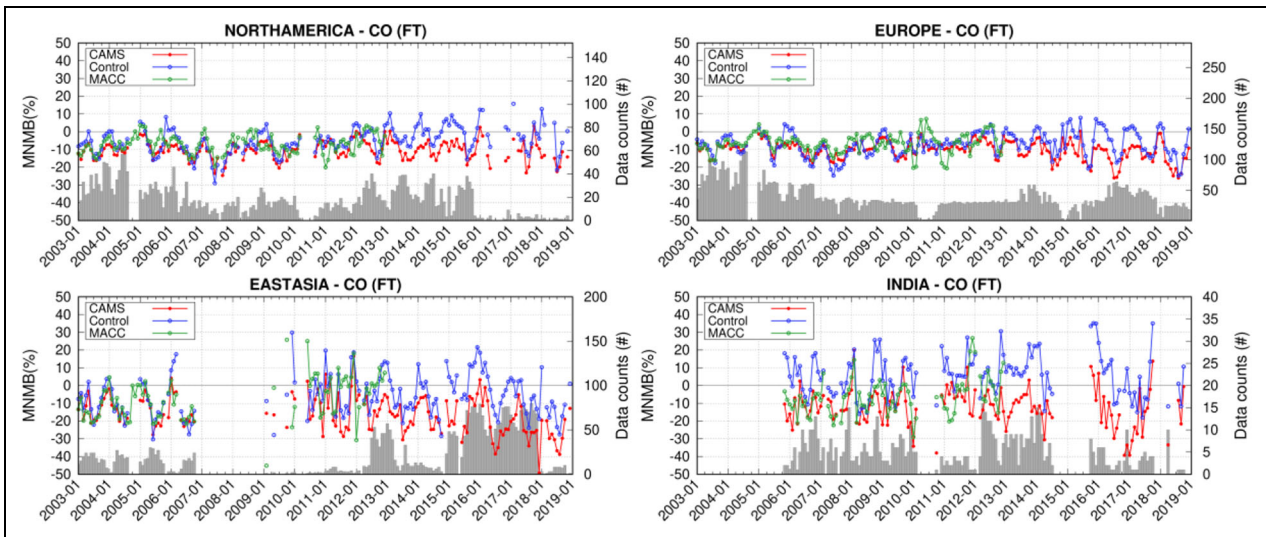
Figure 14. Time series of monthly MNMBs (%) from the comparison against In-service Aircraft for a Global Observing System CO aircraft data in the free troposphere for the period 2003–2018. Top left: North America, top right: Europe, bottom left: East Asia, bottom right: India. The plots show averages over various airports in the free troposphere (350–850 hPa; CAMS reanalysis: red, control run: blue, and MACC reanalysis: green). MNMBs = modified normalized mean biases; CAMS = Copernicus Atmosphere Monitoring Service; MACC = Monitoring Atmospheric Composition and Climate; CO = carbon monoxide. DOI: https://doi.org/10.1525/elementa.2020.00171.f14
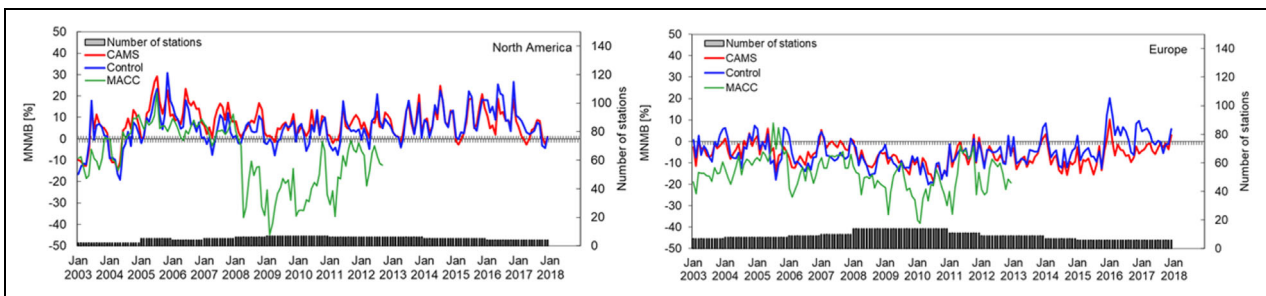
Figure 15. Time series of monthly MNMBs from the comparison against CO Global Atmosphere Watch surface observations. Top left: North America, top right: Europe between 2003 and 2018 (CAMS reanalysis: red, control run: blue, MACC reanalysis: green). MNMBs = modified normalized mean biases; CAMS = Copernicus Atmosphere Monitoring Service; MACC = Monitoring Atmospheric Composition and Climate; JJA = June to August; CO = carbon monoxide. DOI: https://doi.org/10.1525/elementa.2020.00171.f15

China, where various bottom-up inventories likewise cannot capture reduction trends in emissions especially after 2010. Moreover, the MACCity emission inventory has not been updated after 2010, and recent years are only based on projections of past trends.

Next to anthropogenic and fire emissions, another source for CO lies in the oxidation of biogenic VOC emissions as mentioned before. The annual variability in CO biases in the control run closely resembles the annual variation of the MEGAN-MACC isoprene emissions (see Sindelarova et al., 2014; Sindelarova, 2018; Figure 3), with low values during the La Niña year 2008 and an increase during the years after up until the El Nino year 2015/2016. Further investigations, including sensitivity tests, are needed to thoroughly disentangle the specific influence of the different emission sources on the variability and drifts of the biases in the control run.

For most regions shown in **Figure 12**, the biases remain stable for the CAMS reanalysis, which clearly illustrates how well assimilated MOPITT data manages to constrain modeled CO and thus successfully prevents drifts caused by the emissions. This underlines the importance of a stable and consistent satellite CO product for assimilation. Only for East Asia, a drift in bias visibly remains in the CAMS reanalysis (**Figure 12**).

The big fire events in 2003, 2008, and 2012 over Siberia could be captured correctly by the model (Figure S23). In the control run, the magnitude of the events is mostly slightly overestimated, which points to an overestimation of the fire emissions during these events. Autumn and winter 2015/2016 is the period with the largest positive biases. Especially over Asia, autumn 2015 is an exceptional season with increased biases of up to +10%. September and October 2015 were marked by a strong El Niño event, which intensified during the dry season over large regions
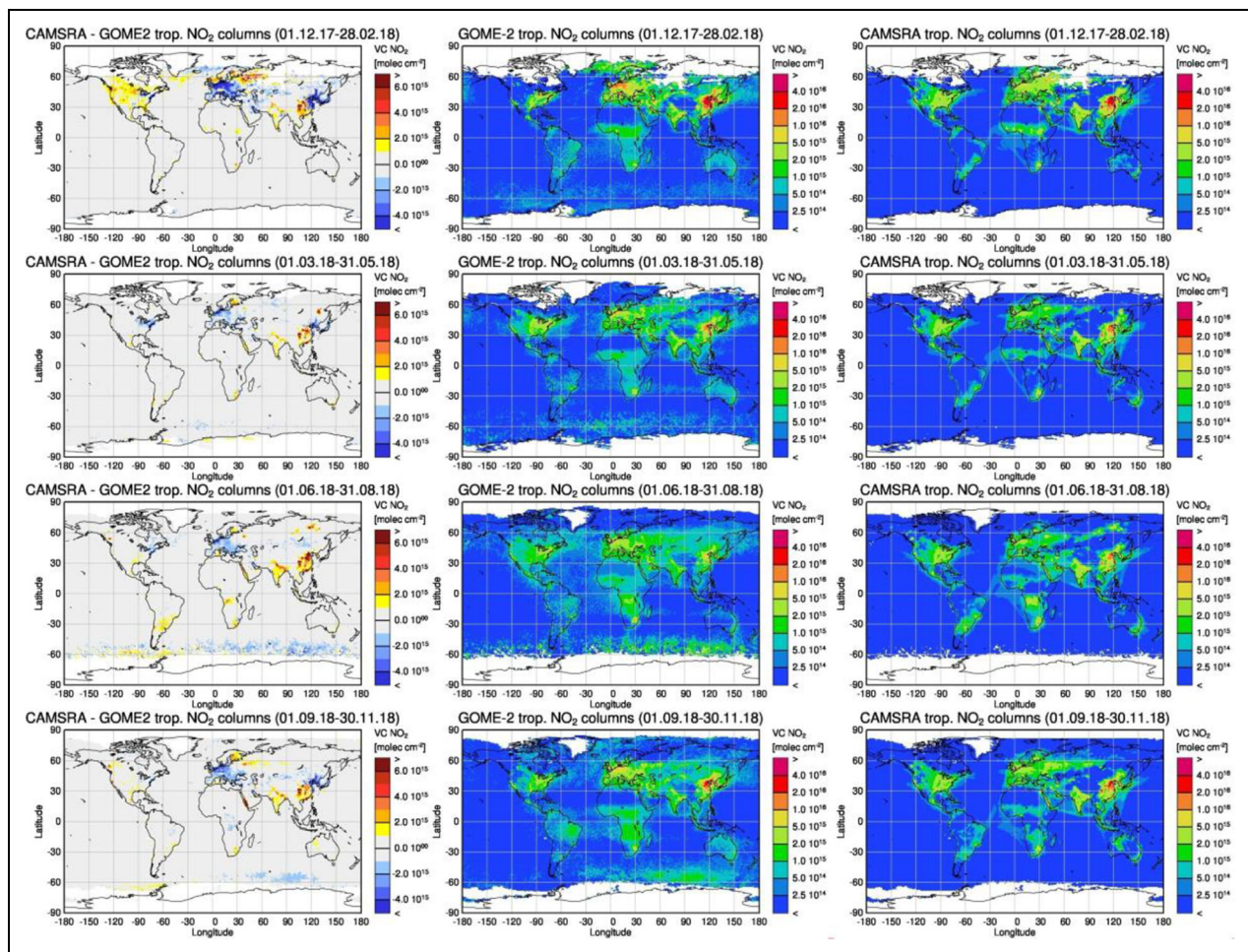
Figure 16. Global map comparisons of satellite-retrieved and model-simulated seasonally averaged tropospheric NO$_2$ columns (molecule cm^{-2}). From top to bottom: DJF 2017/2018, MAM 2018, JJA 2018, and SON 2018. The difference between CAMS reanalysis and GOME-2 is shown in the left, GOME-2 in the middle, and the CAMS reanalysis in the right column. GOME-2 data were gridded to model resolution (i.e., 0.75° × 0.75°). Model data were treated with the same reference sector subtraction approach as the satellite data. SON = September to November; DJF = December to February; MAM = March to May; JJA = June to August; NO$_2$ = nitrogen dioxide; CAMS = Copernicus Atmosphere Monitoring Service; GOME = Global Ozone Monitoring Experiment. DOI: https://doi.org/10.1525/elementa.2020.00171.f16

of Indonesia. During these months, the largest amount of fire emissions were recorded in Indonesia since 1997 based on GFED emissions time series (Huijnen et al., 2016b). The overestimation of emissions during December to March is strongly present in the control run especially for South Asia but could be greatly reduced by the data assimilation.

Figure 13 and Table S9 show relative differences of model and Fourier-transform infrared (FTIR) partial columns (NDACC) for different sites and latitudes. The results for the control run accordingly show the large positive error in the SH and the drifts toward positive biases from 2011 onward for the Northern midlatitudes as described in the validation with satellite data before. The relative differences for the stations in the SH show a significant positive trend in the relative biases: Maido: +0.7%, Lauder: +0.2%, and Wollongong: +1.1% (Figure S25). A negative trend at the Antarctic station Arrival Heights is likely related to the observations, which are dropping in 2009

(Figure S25). For FTIR stations located in the United States and Europe, the validation reveals an underestimation of modeled CO partial columns with values fluctuating around −5% and smaller (Toronto). For Jungfraujoch, Zugspitze, and Toronto, the largest underestimation of CO appears during the summer months (JJA) when CO is low, with values of up to 4% lower compared to the relative bias during the winter months. For three Arctic sites (Eureka, Ny Alesund, and Thule), CO partial columns are slightly underestimated by the model in the order of −5%, which is close to the reported measurement systematic uncertainty. For all three Arctic sites, the strongest underestimation (up to −10%) takes place during the end of winter (January to February, with only few measurements due to polar night) and early spring (March to April). For three sites located in the low latitudes of the NH (Izana, Mauna Loa, and Altzomoni) and five sites in the SH results show that the data assimilation mostly corrects the positive biases in the control run. For some sites (Alzomi and
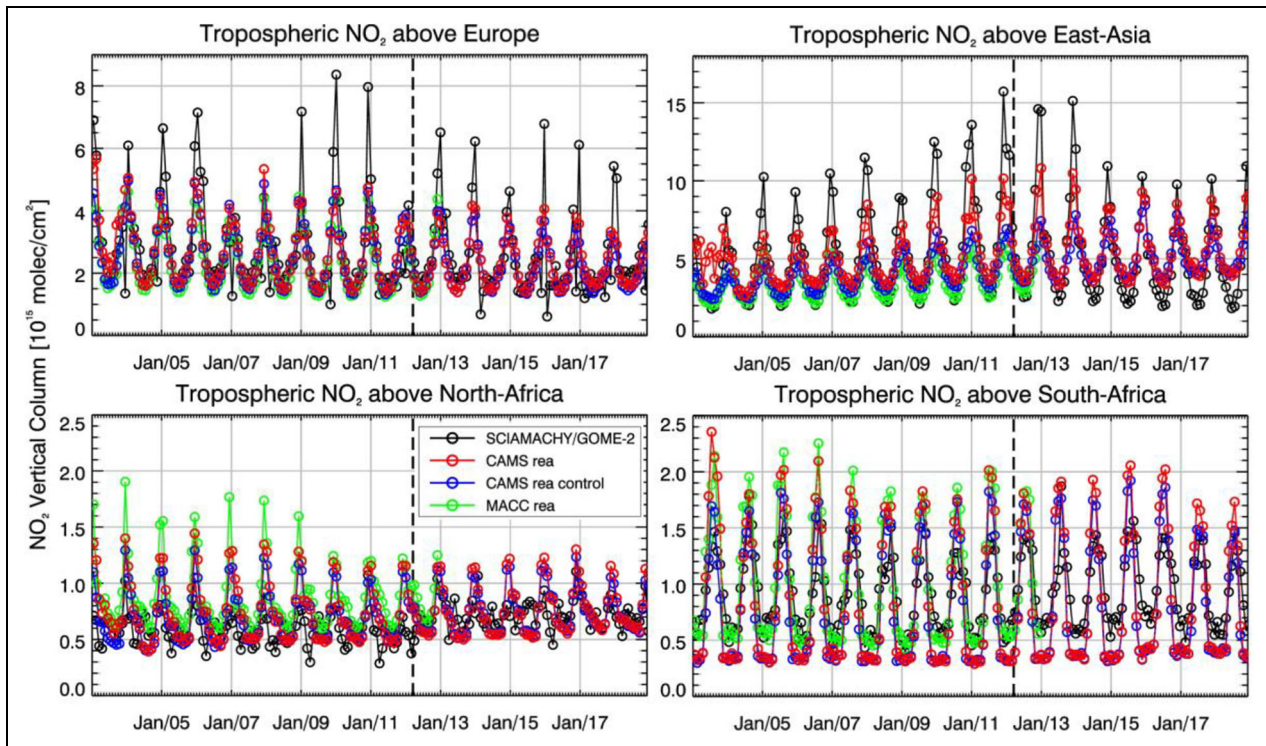
Figure 17. Comparison of time series of tropospheric NO_2 columns from SCIAMACHY and GOME-2 to model results. Tropospheric NO_2 columns (black), CAMS reanalysis (red), control (blue), and MACC reanalysis (green) over selected regions (Europe: 35–70°N, 15°W–35°E; East Asia: 20–45°N, 100–142°E; North Africa: 0–20°N, 15°W–45°E; South Africa: 20°S–0°N, 15–45°E) for the period 2003–2018. The switch from SCIAMACHY to GOME-2 in April 2012 is indicated by the vertical black dashed lines. Upper panels represent regions dominated by anthropogenic emissions; lower panels represent those dominated by biomass burning. NO_2 = nitrogen dioxide; SCIAMACHY = Scanning Imaging Absorption Spectrometer for Atmospheric ChartographY; GOME = Global Ozone Monitoring Experiment; CAMS = Copernicus Atmosphere Monitoring Service; MACC = Monitoring Atmospheric Composition and Climate. DOI: https://doi.org/10.1525/elementa.2020.00171.f17

Wollongong), the assimilation overcorrects to negative biases (around −10%). The correlation between the model and observations is very high (between 0.79 and 0.96).

The evaluation with IAGOS aircraft measurements (**Figure 14**; Figures S26 and S27, Table S11) and GAW surface observations (**Figure 15**; Figures S28 and S29) shows that CO mixing ratios in the free troposphere and at the surface are mostly underestimated by the CAMS reanalysis and control run during 2003 until 2013 for both Europe and East Asia. For later years, the control run partly overestimates CO in the free troposphere. For North America, the validation at the surface shows partly positive MNMBs up to 20%–50% (**Figure 15**; Figure S26). Traffic emissions have been scaled during the winter season for North America and Europe (Stein et al., 2014), which improves the biases for the winter period in both regions (Figures S27–S29). However, during the summer season, surface CO is still too low in Europe, which points to too low emissions in the MACCity inventory (accordingly reported by Hassler et al., 2016) or too large CO sinks. The strong overestimation of modeled surface CO over India points to an overestimation of emissions in this region (Figure S26).

Compared to the MACC reanalysis, the CAMS reanalysis is more consistent over time and has reduced biases (**Figures 13–15**; Tables S9–S12). For NDACC stations in the high

northern latitudes (**Figure 13**), the MACC reanalysis has a negative trend in bias from 2008 onward (biases of up to −20%). This is related to discontinuities in the data assimilation of CO satellite data in the MACC reanalysis, namely the assimilation of IASI satellite data in April 2008, which leads to a decrease of CO especially in the high northern latitudes (see also Flemming et al., 2017; Inness et al., 2019). The distinct drop in bias in April 2008 can be noticed accordingly for validations at the surface with GAW data for North America (**Figure 15**). The CAMS reanalysis that assimilates only MOPITT data is more consistent here and thus shows significant improvement. For tropical regions in the Northern Hemisphere (Izana, Mauna Loa, and Altzomoni), the CAMS reanalysis has an increased bias, which is not observed in the MACC run, however. The validation with GAW surface data shows that the MACC reanalysis has a negative offset for surface CO mixing ratios in Europe and North America (see **Figure 15**, GAW; Figure S26, IAGOS), which is likely related to the unrealistically low wintertime road traffic emissions that were still unscaled in the MACC reanalysis (Inness et al., 2013, 2019).

3.5. Nitrogen dioxide
Tropospheric NO_2 columns have been validated with SCIA-MACHY and GOME-2 satellite data (**Figures 16–18**;
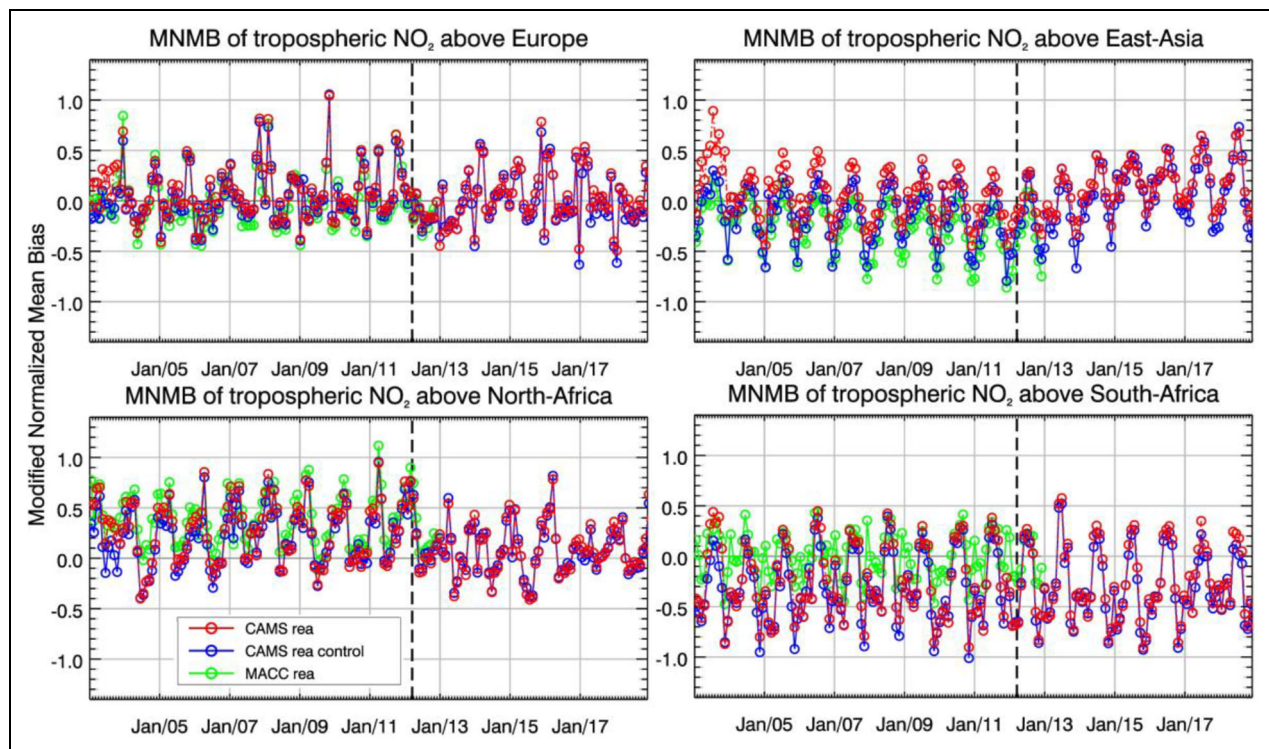
Figure 18. Modified normalized mean bias (MNMB) from the comparison of time series of tropospheric NO_2 columns from SCIAMACHY and GOME-2 to model results. Results are derived from daily averages over a specific region. Negative daily averages of the retrievals have been flagged in the calculation of the MNMB only. NO_2 = nitrogen dioxide; SCIAMACHY = Scanning Imaging Absorption Spectrometer for Atmospheric ChartographY; GOME = Global Ozone Monitoring Experiment. DOI: https://doi.org/10.1525/elementa.2020.00171.f18

Figure S30). Global monthly mean map comparisons show that the spatial distribution of tropospheric NO_2 is overall reproduced well by the CAMS reanalysis (see **Figure 16** as an example of seasonal averages for 2018). However, some differences are apparent between observations and simulations: Simulated shipping signals are generally larger than observed ones, and values over anthropogenic pollution hotspots broadly around the Benelux countries and the German Ruhr area tend to be underestimated (especially in winter), while values over other pollution hotspots are overestimated (e.g., Moscow and Teheran). Boreal forest fire emissions are regularly overestimated over Siberia, Canada, and Alaska mainly from June to August (JJA), and values over fire emission regions are also regularly overestimated in Eastern Russia mainly in April and over South Africa in JJA. The CAMS reanalysis overestimates values over the Persian Gulf and the Red Sea mainly in JJA and SON. Further analysis shows that overestimations of fire emissions do not always occur in both NO_2 and HCHO, especially for boreal forest fires. This difference points to uncertainties regarding fire emission factors, with the results indicating a different performance depending on the trace gas, region, and season.

Time series comparisons based on SCIAMACHY and GOME-2 satellite retrievals are shown in **Figure 17**. Inness et al. (2019) present initial results based on the CAMS reanalysis forecasts for Europe and East Asia. Here, time series of the CAMS analysis results, control run, and MACC reanalysis are shown for East Asia, Europe, North Africa,

and South Africa. Corresponding time series of the MNMB (only positive daily averages are taken into account for the calculation of the MNMB based on the satellite data) are given in **Figure 18**. The CAMS reanalysis reasonably reproduces the magnitude and seasonality in general. Larger differences between the control run and the CAMS reanalysis are apparent only for East Asia. Inness et al. (2019) have shown that CAMS reanalysis forecasts reproduce the satellite-observed increase of wintertime values up to 2014 better than the former MACC reanalysis. This could be the result of assimilating NO_2 from more instruments (with different overpass times) in the CAMS reanalysis, namely, SCIAMACHY, Ozone Monitoring Instrument, and GOME-2. However, maxima are still underestimated by the model. Satellite observations show a strong decrease of wintertime NO_2 over Europe after 2011 and over China after 2014. This tendency is generally captured by the CAMS reanalysis, however, to a lower extent. It shows that control and CAMS reanalysis are closer to each other than in previous years. For summer NO_2, the model does not reproduce the decreasing trend visible for the satellite observations from 2011 onward. Especially for East Asia, values in the model increase instead (see **Figure 18**). In the time series of MNMBs, an increasing trend in MNMBs of CAMS reanalysis and control can thus be noticed for both, for maxima in winter and minima in summer, most clearly seen for East Asia. This trend likely originates from unrealistic emission trends in the model. Another issue appears in 2003: The CAMS reanalysis (in contrast to the
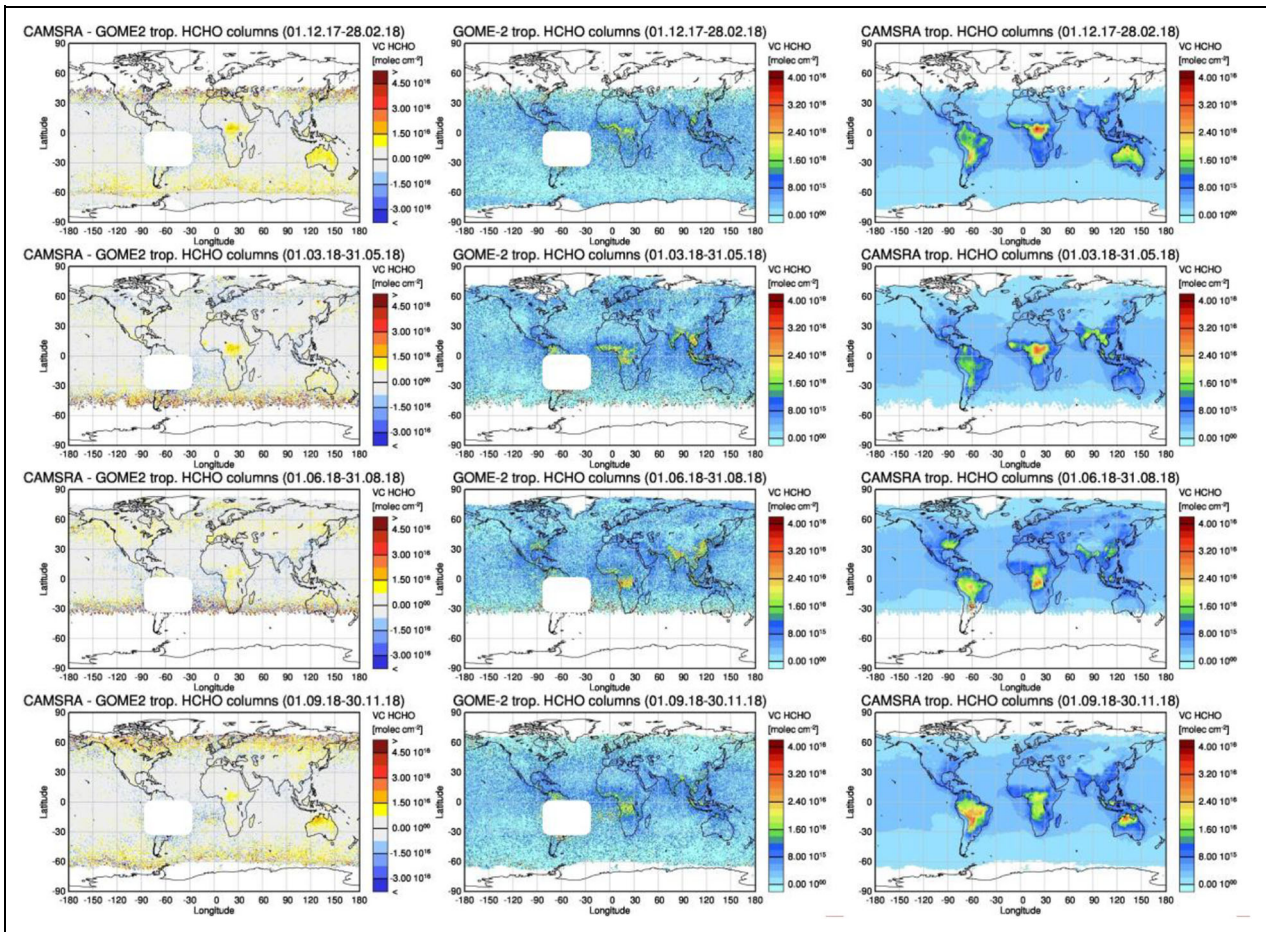
Figure 19. Global map comparisons of satellite-retrieved and model-simulated seasonally averaged tropospheric HCHO columns (molecule cm^{-2}). Satellite-retrieved values in the region of the South Atlantic anomaly are not valid and therefore masked out (white boxes in all images except those that show model results only). HCHO = formaldehyde. DOI: https://doi.org/10.1525/elementa.2020.00171.f19

control run) shows a strong variation of values from 1 month to another and fails to reproduce the observed seasonality due to assimilation of degraded quality NO$_2$ data described in Inness et al. (2019). The seasonal cycle (**Figure 17**) is partly underestimated over Europe, related to the underestimation of values over Central European pollution hotspots described above. The CAMS reanalysis overestimates the seasonal cycle over South Africa, with an underestimation of values around December to April (by about 0.2 × 10^{15} molecule cm^{-2}) and an overestimation of values by about 0.5 × 10^{15} molecule cm^{-2} around JJA (the latter was not present in the MACC reanalysis), which is probably related to an overestimation of fire emissions in this region. As for South Africa, the seasonal cycle is overestimated for North Africa as well, but mainly because of an overestimation of values around December, which, however, improves for the last years of the time series (see also **Figure 18**). The control run is closer to satellite-retrieved maxima over both regions in Africa (dominated by fire emissions) and vice versa over Europe and East Asia (dominated by anthropogenic emissions). Interannual variations are not always captured by the CAMS model. For Europe, reduced satellite-observed NO$_2$ columns are clearly noticeable over Europe during

winter 2007 and 2008, while the simulations do not show a reduction.

Figure S30 shows climatological monthly averages of the MNMB for each region. The monthly MNMB shows little variation from year to year, reflected by low standard deviations. The absolute value of the MNMB of the CAMS reanalysis is in general largest over North Africa around April, over East Asia and South Africa in JJA, and over Europe from October to January. Offsets between the CAMS reanalysis, CAMS control, and MACC reanalysis are visible for East Asia with the CAMS model runs showing smaller absolute values of the MNMB throughout the year. Further offsets are found for North Africa and South Africa.

3.6. Formaldehyde

Tropospheric HCHO columns have been validated with SCIAMACHY and GOME-2 satellite data (**Figures 19–21**; Figure S31). Global monthly mean map comparisons (see **Figure 19** as an example of seasonal averages for 2018) to satellite retrievals from SCIAMACHY and GOME-2 show that the magnitude of oceanic and continental background values and the overall spatial distribution are well represented by the CAMS reanalysis. Compared to SCIAMACHY and GOME-2 satellite retrievals, there is an
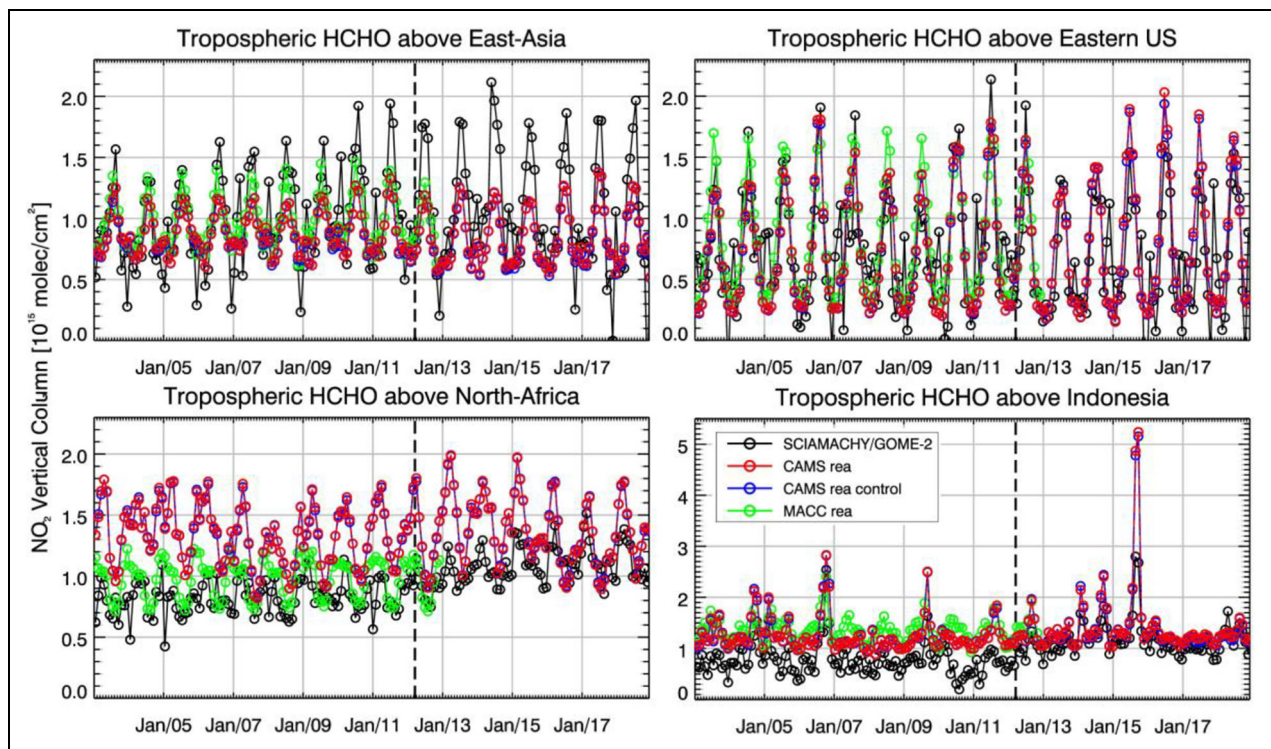
Figure 20. Comparison of time series of tropospheric HCHO columns from SCIAMACHY (up to April 2012) and GOME-2 (from April 2012 onward) to model results (HCHO columns: black, CAMS reanalysis: red, control: blue, and MACC reanalysis: green). The switch from SCIAMACHY to GOME-2 in April 2012 is indicated by the vertical black dashed lines. The regions differ from those used for NO_2 shown in **Figure 17** to better focus on HCHO hotspots: East Asia: 25–40°N, 110–125°E; Eastern United States: 30–40°N, 75–90°W; Northern Africa: 0–15°N, 15°W–25°E; and Indonesia: 5°S–5°N, 100–120°E. Negative satellite-retrieved values over Eastern United States are due to a lack of data during the Northern Hemisphere winter months for this region. HCHO = formaldehyde; SCIAMACHY = Scanning Imaging Absorption Spectrometer for Atmospheric ChartographY; GOME = Global Ozone Monitoring Experiment; CAMS = Copernicus Atmosphere Monitoring Service; MACC = Monitoring Atmospheric Composition and Climate; NO_2 = nitrogen dioxide. DOI: https://doi.org/10.1525/elementa.2020.00171.f20

overestimation of values over regions with fire activity in Central Africa mainly in DJF/MAM and over Eastern Russia around April, as well as over regions with fire and biogenic emissions in Northern Australia mainly during SON and DJF. As there is no HCHO data assimilated, there is only a little difference between CAMS reanalysis and control run for HCHO in general. Time series comparisons are shown in **Figure 20** for selected regions, together with the MNMBs in **Figure 21** (only positive daily averages are taken into account for the calculation of the MNMB based on the satellite data). East Asia and the Eastern United States are considered as regions dominated by biogenic emissions with some anthropogenic input. The CAMS reanalysis reproduces satellite observations for Eastern United States with respect to absolute values and seasonality but does not match the maxima of the satellite retrievals for individual years. Seasonality over East Asia is generally underestimated with differences of up to approximately 1×10^{15} molecule cm^{-2} shown in the time series, the MACC reanalysis is closer to satellite-retrieved HCHO columns than the CAMS reanalysis here. For the regions North Africa and Indonesia, which are dominated by biogenic and pyrogenic sources, the reanalysis runs show a positive offset compared to satellite retrievals. The

seasonality is in agreement with the retrievals for Indonesia and overestimated for North Africa. For September and October 2015 over Indonesia, satellite retrievals and simulations show a distinct maximum, which is, however, much more pronounced in the simulations. September, October, and November 2015 were strong El Nino months (e.g., NOAA El Niño webpage), which caused droughts and higher fire activity in Indonesia. Fire emissions used by the CAMS reanalysis seem to be largely overestimated for this El Nino year, resulting in an overestimation of up to a factor of 1.8 compared to the observations. A similar overestimation was also reported for the CAMS NRT product, for which it was shown that this is not due to cloud flagging applied to the satellite and model data (Huijnen et al., 2016a). Note that weaker El Nino conditions occurred for periods in 2006 and 2009, which resulted in maxima in the satellite-retrieved values that are reproduced for 2006 but again overestimated for 2009. Figure S31 shows climatological monthly averages of the MNMB for each region. A seasonal cycle of the MNMB is only found for Eastern United States, with values around –0.9 in DJF and about 0.2 from spring to autumn for the CAMS reanalyses. As for NO_2, the monthly MNMB shows little variation from year to year (low standard deviations).
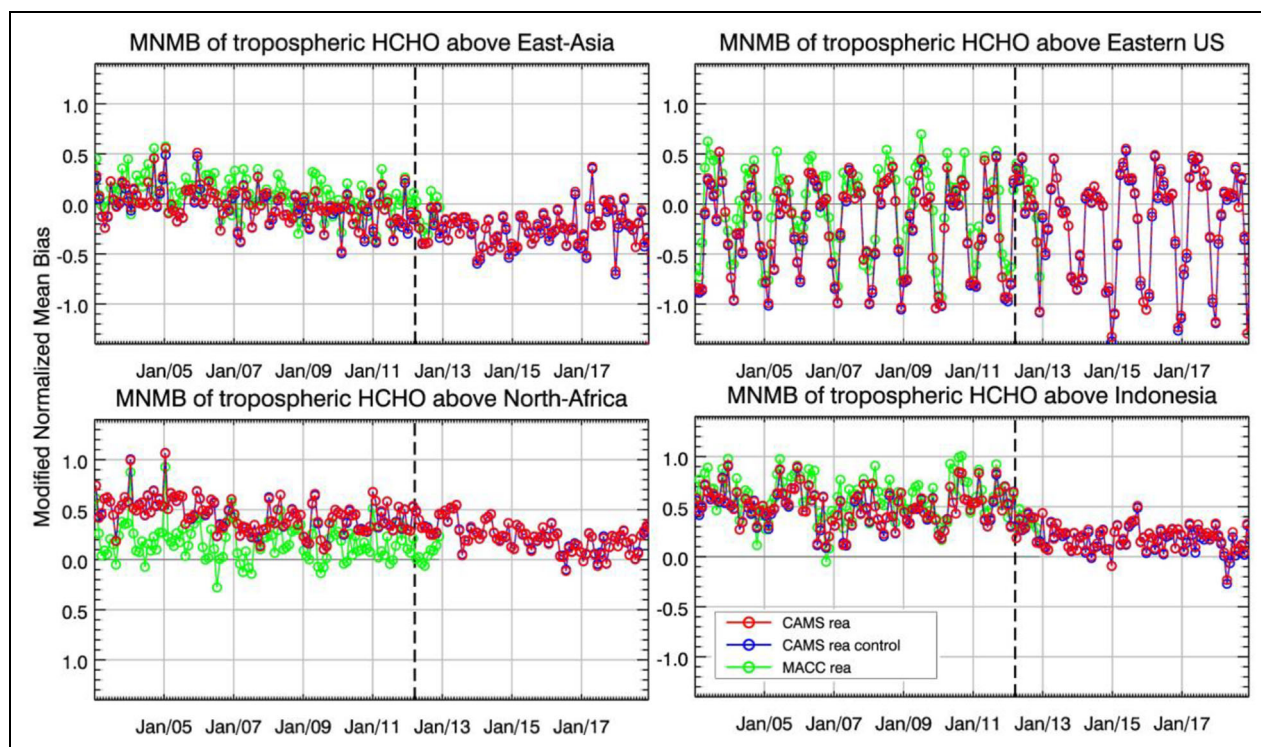
Figure 21. Time series of MNMBs (derived from daily averages) from the comparison of tropospheric HCHO columns from SCIAMACHY (up to April 2012) and GOME-2 (from April 2012 onward) to model results (CAMS reanalysis: red, control: blue, and MACC reanalysis: green). Negative daily averages of the retrievals have been flagged in the calculation of the MNMB only. MNMBs = modified normalized mean biases; HCHO = formaldehyde; SCIAMACHY = Scanning Imaging Absorption Spectrometer for Atmospheric ChartographY; GOME = Global Ozone Monitoring Experiment; CAMS = Copernicus Atmosphere Monitoring Service; MACC = Monitoring Atmospheric Composition and Climate; MNMB = modified normalized mean bias. DOI: https://doi.org/10.1525/elementa.2020.00171.f21

Comparison with the MACC reanalysis shows that the CAMS reanalysis has lower MNMBs for Indonesia and East Asia during the summer period (Figure S31), likely related to the differences in the fire emissions used (GFED/GFAS v0 in MACC and GFAS v1.2 in CAMS). For other regions and periods, the CAMS reanalysis results in larger MNMBs.

4. Conclusions

CAMS provides its users with a variety of different products in the field of air quality and AC. Beside the NRT forecasts, there is also a large and growing interest in long-term retrospective analysis (reanalysis) data sets. After the release of the MACC reanalysis in 2013, and an interim test product in 2015, CAMS has now produced a new reanalysis data set (CAMS reanalysis), which is freely available to the public.

We have comprehensively validated the reactive gas species (O_3, CO, NO_2, and HCHO) of this new product in the period 2003–2018 with multiple independent observations. For reanalysis data sets, a temporal stability of the model results over time is crucial, for example, for trend studies on chemical species. Special focus was thus set on the long-term consistency shown in the time series of biases and on the assessment of seasonal and interseasonal changes in biases. In order to thoroughly evaluate the impact of data assimilation on the long-term quality of results, a comparison with a control run without assimilated data is conducted. Finally, improvements and shortcomings of the CAMS reanalysis compared to the previous MACC reanalysis are quantified and discussed.

Our evaluations show that the CAMS reanalysis reproduces O_3 with MNMBs mostly within $\pm 10\%$ in the stratosphere and troposphere of the Northern midlatitudes compared to sonde observations and satellite instruments. Larger biases (up to $\pm 38\%$) appear over the high latitudes, the Tropics, and generally for surface O_3. Total column CO over Europe, the United States, East Asia, and North Africa is reproduced with MNMBs mostly within $\pm 10\%$. Larger MNMBs appear over East Asia and for surface CO, reaching up to $\pm 40\%$. The CAMS reanalysis performs reasonably well regarding the magnitude and seasonality of NO_2 in comparison with SCIAMACHY and GOME-2 NO_2 satellite retrievals. Stronger shipping signals show up compared to the satellite observations, and NO_2 in boreal fire regions is overestimated in summer, whereas NO_2 over the pollution hotspots of Central Europe is underestimated in winter. Modeled HCHO columns mostly show a good agreement with SCIAMACHY and GOME-2 satellite observations. For regions dominated by biogenic emissions with some anthropogenic input (East Asia and Eastern United States), the CAMS reanalysis reproduces absolute values and seasonality but fails to match the maxima of the satellite retrievals for individual years. The seasonality over East Asia is generally underestimated

with differences of up to approximately 1×10^{15} molecule cm^{-2}. For regions where biogenic and pyrogenic sources dominantly influence HCHO columns (North Africa and Indonesia), the CAMS reanalysis shows a positive offset compared to satellite retrievals. Concerning the long-term consistency, our results show that the CAMS model system mostly provides a stable and accurate representation of the global distribution of reactive gases over time.

However, the comparison with the control without data assimilation reveals some shortcomings in the model and emissions: The lack of an explicit modeling of stratospheric chemistry leads to large biases for stratospheric O_3. For tropospheric and surface O_3, the model shows seasonal patterns in the biases in midlatitude and high-latitude regions with larger negative MNMBs during winter and spring. For the Arctic, large positive biases appear during O_3 depletion events in spring. Furthermore, the control run shows large overestimation for CO in the SH, likely related to the overestimation of fire and biogenic emissions, together with shortcomings in the simulation of the global loss, production, and large-scale transport of CO. Overestimations of HCHO concentrations likewise suggest that fire emissions are overestimated over boreal regions, Indonesia, Africa, and East Asia, especially during years with high fire activity like during the strong El Niño event 2015/2016.

Finally, we also discovered positive drifts in the inter-annual time series of biases for various species (CO, O_3, and NO_2) in the control run, likely triggered by unrealistic emission trends, especially after 2010. Data assimilation is able to successfully constrain stratospheric and tropospheric O_3 and CO and thus ensures the long-term consistency and stability of the CAMS reanalysis. However, this works less effectively near the surface and for short-lived species like NO_2.

Our evaluations concerning the long-term stability of the CAMS reanalysis show that the consistency in the quality of model results is also essentially affected by limitations in the availability of high-quality data for assimilation and by changes in the assimilated satellite data sets. Especially during the first years, degraded quality data and the lack of O_3 profile data deteriorated the validation results for O_3 and NO_2. Modifications in the assimilation system in 2012/2013 cause jumps in the interannual seasonal time series of biases for tropospheric and surface O_3, especially over high-latitude regions. For trend analysis, these effects related to changes in the data assimilation need to be considered and removed.

Compared to the MACC reanalysis, the CAMS reanalysis has systematically lower biases, better correlation, and a weaker seasonal pattern for O_3 especially in the free troposphere and at the surface. Aside from the improved data assimilation, especially the change in the chemistry module, that is, the online-coupled IFS model combined with the different chemistry treatment in the CB05 model leads to a reduction of biases for tropospheric and surface O_3. Largest improvement in the magnitude of biases is thus found over the Arctic and Antarctic regions. For CO, the comparison with the MACC reanalysis shows that the scaling of the winter road traffic emissions and a more

consistent data assimilation improve the results. For NO_2, the CAMS reanalysis shows a better reproduction of wintertime NO_2 over East Asia. For South Africa, however, the CAMS reanalysis has larger underestimations of observed NO_2 during SH summer and autumn. For HCHO, improvements compared to the MACC reanalysis can be seen over Indonesia, but for North Africa and the Eastern United States, the MACC reanalysis shows smaller biases.

For next-generation CAMS reanalyses, challenges in the data assimilation will include the integration of more species (e.g., HCHO) and additional sensors (O_3 profile data turned out to have a crucial impact) while assuring good long-term stability of results. New sensors such as sentinel 5P will provide promising perspectives. Our results concerning the control run suggest that deficiencies in the model's chemistry and transport scheme need to be investigated and improved further, especially in combination with the emission data sets, to remove large zonal errors such as the overestimation of CO in the SH as well as drifts and seasonal patterns in the biases of the control run. Given the large impact of anthropogenic, fire, and biogenic emissions on CO, more care should be taken to investigate and consolidate emission rates and trends. Simple scaling approaches as conducted for the wintertime traffic emissions could be replaced by more sophisticated approximations, available from recent bottom-up and top-down inventories. A more comprehensive stratospheric chemistry scheme could improve the model results in the stratosphere. Furthermore, the integration of small-scale local processes, such as halogen chemistry, could help to reduce more local sources of errors in the model system, such as the large biases for surface O_3 over the Arctic in springtime.

Data accessibility statement
Bennouna et al. (2020): Validation report of the CAMS global Reanalysis of aerosols and reactive gases, years 2003–2019, Copernicus Atmosphere Monitoring Service (CAMS) report: Available at CAMS84_2018SC2_D5.1.1-2019.pdf, Accessed 4 May 2021, DOI: http://dx.doi.org/10.24380/2v3p-ab79.

The CAMS reanalysis data set that was not produced in the frame of our study but as a product of CAMS can be found at Atmosphere Data Store. Available at https://ads.atmosphere.copernicus.eu. Accessed 4 May 2021.

Supplemental files
The supplemental files for this article can be found in a composite file (docx).

Acknowledgments

Funding

Competing interests
The authors have declared that no competing interests exist.

Author contributions
Contributed to conception and design: AW, YB, AMB, SC, YC, QE, KMH, JK, BL, NS.

Contributed to acquisition of data: JF, AI, AR, VT.

Contributed to analysis and interpretation of data: AW, YB, AMB, SC, YC, KMH, JK, BL, NS, CZ.

Drafted and/or revised the article: AW, SB, YB, AMB, GB, SC, YC, QE, HE, JE, AI, KMH, JK, ZK, BL, MS, NS.

Approved the submitted version for publication: AW, YB, AMB, GB, SC, YC, QE, HE, JF, KMH, AI, JK, BL, AR, NS, VT, CZ.

References

Aas, W, Hjellbrekke, A-G, Schaug, J, Solberg S. 2001. Data quality 1999, quality assurance, and field comparisons. EMEP/CCC-Report 6/2001. Kjeller, Norway: Norwegian Institute for Air Research. Available at https://projects.nilu.no/ccc/reports/cccr6-2001.pdf. Accessed 4 May 2021.

Bechtold, P, Orr, A, Morcrette, JJ, Engelen, R, Flemming, J, Janiskova, M. 2009, Summer. Improvements in the stratosphere and mesosphere of the IFS. *ECMWF Newsletter* **120**: 22–31.

Benedetti, A, Jones, L, Kaiser, JW, Morcrette, JJ, Rémy, S. 2014. Global climate, aerosols: In State of the Climate in 2013. *American Meteorological Society* **95**: 36–37.

Benedetti, A, Morcrette, J-J, Boucher, O, Dethof, A, Engelen, RJ, Fisher, M, Flentje, H, Huneeus, N, Jones, L, Kaiser, JW, Kinne, S, Mangold, A, Razinger, M, Simmons, AJ, Suttie, M, GEMS-AER Team. 2009. Aerosol analysis and forecast in the European Centre for Medium-Range Weather Forecasts Integrated Forecast System: 2. Data assimilation. *Journal of Geophysical Research* **114**: D13205. DOI: http://dx.doi.org/10.1029/2008JD011115.

Bennouna, Y, Christophe, Y, Schulz, MY, Christophe, HJ, Eskes, S, Basart, A, Benedictow, A-M, Blechschmidt, S, Chabrillat, H, Clark, E, Cuevas, H, Flentje, KM, Hansen, UIM, Kapsomenakis, J, Langerock, B, Petersen, K, Richter, A, Sudarchikova, N, Thouret, V, Wagner, A, Wang, Y, Warneke, T, Zerefos, C. 2020. Validation report of the CAMS global reanalysis of aerosols and reactive gases, years 2003–2019. Copernicus Atmosphere Monitoring Service (CAMS) report. CAMS84_2018SC2_D5.1.1-2019.pdf. DOI: http://dx.doi.org/10.24380/2v3p-ab79.

Bozzo, A, Benedetti, A, Flemming, J, Kipling, Z, Rémy, S. 2020. An aerosol climatology for global models based on the tropospheric aerosol scheme in the Integrated Forecasting System of ECMWF. *Geoscientific Model Development* **13**: 1007–1034. DOI: http://dx.doi.org/10.5194/gmd-13-1007-2020.

CAMS Atmosphere Data Store. Available at https://ads.atmosphere.copernicus.eu. Accessed 4 May 2021.

CAMS Confluence. Available at https://confluence.ecmwf.int/display/CKB/CAMS%3A+Reanalysis+data+documentation. Accessed 4 May 2021.

Cariolle, D, Teyssèdre, H. 2007. A revised linear ozone photochemistry parameterization for use in transport and general circulation models: Multi-annual simulations. *Atmospheric Chemistry and Physics* **7**:

2183–2196. DOI: http://dx.doi.org/10.5194/acp-7-2183-2007.

Cuevas, E, Camino, C, Benedetti, A, Basart, S, Terradellas, E, Baldasano, JM, Morcrette, JJ, Marticorena, B, Goloub, P, Mortier, A, Berjón, A, Hernández, Y, Gil-Ojeda, M, Schulz, M. 2015. The MACC-II 2007–2008 reanalysis: Atmospheric dust evaluation and characterization over Northern Africa and the Middle East. *Atmospheric Chemistry and Physics* **15**: 3991–4024. DOI: http://dx.doi.org/10.5194/acp-15-3991-2015.

Deeter, MN, Edwards, DP, Francis, GL, Gille, JC, Martinez-Alonso, S, Worden, HM, Sweeney, C. 2017. A climate-scale satellite record for carbon monoxide: The MOPITT Version 7 product. *Atmospheric Measurement Techniques* **10**: 2533–2555.

DeMazière, M, Thompson, A, Kurylo, M, Wild, J, Bernhard, G, Blumenstock, T, Braathen, G, Hannigan, J, Lambert, J-C, Leblanc, T, McGee, T, Nedoluha, G, Petropavlovskikh, I, Seckmeyer, G, Simon, P, Steinbrecht, W, Strahan, S. 2018. The network for the detection of atmospheric composition change (NDACC): History, status and perspectives Atmos. *Chemical Physics* **18**: 4935–4964. DOI: http://dx.doi.org/10.5194/acp-18-4935-2018.

Deshler, T, Mercer, JL, Smit, HGJ, Stubi, R, Levrat, G, Johnson, BJ, Oltmans, SJ, Kivi, R, Thompson, AM, Witte, J, Davies, J, Schmidlin, FJ, Brothers, G, Sasaki, T. 2008. Atmospheric comparison of electrochemical cell ozonesondes from different maufacturers, and with different cathode solution strengths: The Balloon Experiment on Standards for Ozonsondes. *Journal of Geophysical Research* **113**: D04307. DOI: http://dx.doi.org/10.1029/2007JD008975.

Elguindi, N, Granier, C, Stavrakou, T, Darras, S, Bauwens, M, Cao, H, Chen, C, Denier van der Gon, HAC, Dubovik, O, Fu, TM, Henze, DK, Jiang, Z, Keita, S, Kuenen, JJP, Kurokawa, J, Liousse, C, Miyazaki, K, Müller, J-F, Qu, Z, Solmon, F, Zheng, B. 2020. Intercomparison of magnitudes and trends in anthropogenic surface emissions from bottom-up inventories, top-down estimates, and emission scenarios. *Earth's Future* **8**: e2020EF001520. DOI: http://dx.doi.org/10.1029/2020EF001520.

Errera, Q, Chabrillat, S, Christophe, Y, Debosscher, J, Hubert, D, Lahoz, W, Santee, ML, Shiotani, M, Skachko, S, von Clarmann, T, Walker, K. 2019. Technical note: Reanalysis of Aura MLS chemical observations. *Atmospheric Chemistry and Physics* **19**: 13647–13679. DOI: http://dx.doi.org/10.5194/acp-19-13647-2019.

Eskes, HJ, Basart, S, Benedictow, A, Bennouna, Y, Blechschmidt, A-M, Chabrillat, S, Christophe, Y, Cuevas, E, Douros, J, Flentje, H, Hansen, KM, Kapsomenakis, J, Langerock, BM, Ramonet, M, Richter, A, Schulz, M, Sudarchikova, N, Wagner, A, Warneke, T, Zerefos, C. 2018. Observations characterisation and validation methods document. Copernicus Atmosphere Monitoring Service (CAMS)

report. 1–71 October 2018, in Eskes, HJ, Douros, J eds., CAMS84_2015SC3_D.84.8.1.1-2018_observations_v3.pdf. Available at https://atmosphere.copernicus.eu/sites/default/files/2018-12/CAMS84_2015SC3_D.84.8.1.1-2018_observations_v3.pdf. Accessed 4 May 2021.

Eskes, H, Huijnen, V, Arola, A, Benedictow, A, Blechschmidt, A-M, Botek, E, Boucher, O, Bouarar, I, Chabrillat, S, Cuevas, E, Engelen, R, Flentje, H, Gaudel, A, Griesfeller, J, Jones, L, Kapsomenakis, J, Katragkou, E, Kinne, S, Langerock, B, Razinger, M, Richter, A, Schultz, M, Sudarchikova, N, Thouret, V, Vrekoussis, M, Wagner, A, Zerefos, C. 2015. Validation of reactive gases and aerosols in the MACC global analysis and forecast system. *Geoscientific Model Development* **8**: 3523–3543. DOI: http://dx.doi.org/10.5194/gmd-8-3523-2015.

Flemming, J, Benedetti, A, Inness, A, Engelen, RJ, Jones, L, Huijnen, V, Remy, S, Parrington, M, Suttie, M, Bozzo, A, Peuch, V-H, Akritidis, D, Katragkou, E. 2017. The CAMS interim reanalysis of carbon monoxide, ozone and aerosol for 2003–2015. *Atmospheric Chemistry and Physics* **17**: 1945–1983. DOI: http://dx.doi.org/10.5194/acp-17-1945-2017.

Flemming, J, Huijnen, V, Arteta, J, Bechtold, P, Beljaars, A, Blechschmidt, A-M, Diamantakis, M, Engelen, RJ, Gaudel, A, Inness, A, Jones, L, Josse, B, Katragkou, E, Marecal, V, Peuch, V-H, Richter, A, Schultz, MG, Stein, O, Tsikerdekis, A. 2015. Tropospheric chemistry in the integrated forecasting system of ECMWF. *Geoscientific Model Development* **8**, 975–1003. DOI: http://dx.doi.org/10.5194/gmd-8-975-2015.

Flemming, J, Inness, A. 2019. Carbon monoxide: In State of the Climate in 2018. *Bulletin of the American Meteorological Society* **100**(9): S181–S185. DOI: http://dx.doi.org/10.1175/2019BAMSStateoftheClimate.1.

Gaubert, B, Emmons, LK, Raeder, K, Tilmes, S, Miyazaki, K, Arellano Jr, AF, Elguindi, N, Granier, C, Tang, W, Barré, J, Worden, HM, Buchholz, RR, Edwards, DP, Franke, P, Anderson, JL, Saunois, M, Schroeder, J, Woo, J-H, Simpson, IJ, Blake, DR, Meinardi, S, Wennberg, PO, Crounse, J, Teng, A, Kim, M, Dickerson, RR, He, H, Ren, X, Pusede, SE, Diskin, GS. 2020. Correcting model biases of CO in East Asia: Impact on oxidant distributions during KORUS-AQ. *Atmospheric Chemistry and Physics* **20**: 14617–14647. DOI: http://dx.doi.org/10.5194/acp-20-14617-2020.

George, M, Clerbaux, C, Bouarar, I, Coheur, P-F, Deeter, MN, Edwards, DP, Francis, G, Gille, J, Hadji-Lazaro1, C, Hurtmans, JD, Inness, A, Mao, D, Worden, HM. 2015. An examination of the long-term CO records from MOPITT and IASI: Comparison of retrieval methodology. *Atmospheric Measurement Techniques* **8**: 4313–4328. DOI: http://dx.doi.org/10.5194/amt-8-4313-2015.

George, M, Clerbaux, C, Hurtmans, D, Turquety, S, Coheur, PF, Pommier, M, Hadji-Lazaro, J, Edwards, DP, Worden, H, Luo, M, Rinsland, C, McMillan, W. 2009. Carbon monoxide distributions from the IASI/METOP mission: Evaluation with other space-borne remote sensors. *Atmospheric Chemistry and Physics* **9**: 8317–8330.

Giordano, L, Brunner, D, Flemming, J, Hogrefe, C, Im, U, Bianconi, R, Badia, A, Balzarini, A, Baró, R, Chemel, C, Curci, G, Forkel, R, Jiménez-Guerrero, P, Hirtl, M, Hodzic, A, Honzak, L, Jorba, O, Knote, C, Kuenen, JJP, Makar, PA, Manders-Groot, A, Neal, L, Pérez, JL, Pirovano, G, Pouliot, G, San José, R, Savage, N, Schröder, W, Sokhi, RS, Syrakov, D, Torian, A, Tuccella, P, Werhahn, J, Wolke, R, Yahya, K, Žabkar, R, Zhang, Y, Galmarini, S. 2015. Assessment of the MACC reanalysis and its influence as chemical boundary conditions for regional air quality modelling in AQMEII-2. *Atmospheric Environment* **115**: 371–388.

Granier, C, Bessagnet, B, Bond, T, D'Angiola, Avd, Gon, HD, Frost, GJ, Heil, A, Kaiser, JW, Kinne, S, Klimont, Z, Kloster, S, Lamarque, J-F, Liousse, C, Masui, T, Meleux, F, Mieville, A, Ohara, T, Raut, J-C, Riahi, K, Schultz, MG, Smith, SJ, Thomson, Av, Aardenne, Jvd, Werf, GR, Vuuren, DPv. 2011. Evolution of anthropogenic and biomass burning emissions of air pollutants at global and regional scales during the 1980–2010 period. *Climatic Change* **109**: 163–190. DOI: http://dx.doi.org/10.1007/s10584-011-0154-1.

Hassler, B, Brian, C, McDonald, B, Frost, G, Borbon, A, Carslaw, D, Civerolo, K, Granier, C, Monks, P, Monks, S, Parrish, D, Pollack, I, Rosenlof, K, Ryerson, T, Schneidemesser, E, Trainer, M. 2016. Analysis of long-term observations of NO_x and CO in megacities and application to constraining emissions inventories. *Geophysical Research Letters* **43**: 9920–9930. DOI: http://dx.doi.org/10.1002/2016GL069894.

Huijnen, V, Eskes, HJ, Wagner, A, Schulz, M, Christophe, Y, Ramonet, M, Basart, S, Benedictow, A, Blechschmidt, AM, Chabrillat, S, Clark, H. 2016a. Validation report of the CAMS near-real time global atmospheric composition service system evolution and performance statistics, in Huijnen, V, Eskes, HJ, Schulz, M, Chabrillat, S eds., Status up to 1 December 2015 REF. CAMS84_2015SC1_D.84.1.2-2016Q1_201602. Available at https://atmosphere.copernicus.eu/sites/default/files/repository/CAMS84_2015SC1_D.84.1.2-2016Q1_201602.pdf. Accessed 4 May 2021.

Huijnen, V, Miyazaki, K, Flemming, J, Inness, A, Sekiya, T, Schutz, M. 2020. An intercomparison of tropospheric ozone reanalysis products from CAMS, CAMS interim, TCR-1, and TCR-2. *Geoscientific Model Development* **13**: 1513–1544.

Huijnen, V, Williams, J, van Weele, M, van Noije, T, Krol, M, Dentener, F, Segers, A, Houweling, S, Peters, W, de Laat, J, Boersma, F, Bergamaschi, P, van Velthoven, P, Le Sager, P, Eskes, H, Alkemade, F, Scheele, R, Nédélec, P, Pätz, H-W. 2010. The global chemistry transport model TM5: Description and evaluation of the tropospheric chemistry Version 3.0. *Geoscientific Model Development* **3**: 445–473. DOI: http://dx.doi.org/10.5194/gmd-3-445-2010.

Huijnen, V, Wooster, MJ, Kaiser, JW, Gaveau, DLA, Flemming, J, Parrington, M, Inness, A, Murdiyarso, D, Main, B, van Weele, M. 2016b. Fire carbon emissions over maritime Southeast Asia in 2015 largest since 1997. *Scientific Reports* **6**: 26886. DOI: http://dx.doi.org/10.1038/srep26886.

IAGOS homepage. Available at http://www.iagos.org. Accessed 4 May 2021.

Illingworth, SM, Remedios, JJ, Boesch, H, Ho, S-P, Edwards, DP, Palmer, PI, Gonzi, S. 2011. A comparison of OEM CO retrievals from the IASI and MOPITT instruments. *Atmospheric Measurement Techniques* **4**: 775–793. DOI: http://dx.doi.org/10.5194/amt-4-775-2011.

Im, U, Bianconi, R, Solazzo, E, Kioutsioukis, I, Badia, A, Balzarini, A, Baró, R, Bellasio, R, Brunner, D, Chemel, C, Curci, G, Flemming, J, Forkel, R, Giordano, L, Jiménez- Guerrero, P, Hirtl, M, Hodzic, A, Honzak, L, Jorba, O, Knote, C, Kuenen, JJP, Makar, PA, Manders-Groot, A, Neal, L, Pérez, JL, Pirovano, G, Pouliot, G, San Jose, R, Savage, N, Schroder, W, Sokhi, RS, Syrakov, D, Torian, A, Tuccella, P, Werhahn, J, Wolke, R, Yahya, K, Zabkar, R, Zhang, Y, Zhang, J, Hogrefe, C, Galmarini, S. 2015. Evaluation of operational on-line-coupled regional air quality models over Europe and North America in the context of AQMEII Phase 2, Part I: Ozone. *Atmospheric Environment* **115**: 404–420. DOI: http://dx.doi.org/10.1016/j.atmosenv.2014.09.042.

Inness, A, Ades, M, Agusti-Panareda, A, Barré, J, Benedictow, A, Blechschmidt, AM, Dominguez, J, Engelen, R, Eskes, HJ, Flemming, J, Huijnen, V, Jones, L, Kipling, Z, Massart, S, Parrington, M, Peuch, V-H, Razinger, M, Remy, S, Schulz, M, Suttie, M. 2019. The CAMS reanalysis of atmospheric composition. *Atmospheric Chemistry and Physics* **19**: 3515–3556. DOI: http://dx.doi.org/10.5194/acp-19-3515-2019.

Inness, A, Baier, F, Benedetti, A, Bouarar, I, Chabrillat, S, Clark, H, Clerbaux, C, Coheur, P, Engelen, RJ, Errera, Q, Flemming, J, George, M, Granier, C, Hadji-Lazaro, J, Huijnen, V, Hurtmans, D, Jones, L, Kaiser, JW, Kapsomenakis, J, Lefever, K, Leitão, J, Razinger, M, Richter, A, Schultz, MG, Simmons, AJ, Suttie, M, Stein, O, Thépaut, J-N, Thouret, V, Vrekoussis, M, Zerefos, C, MACC Team. 2013. The MACC reanalysis: An 8 yr data set of atmospheric composition. *Atmospheric Chemistry and Physics* **13**: 4073–4109. DOI: http://dx.doi.org/10.5194/acp-13-4073-2013.

Inness, A, Blechschmidt, A-M, Bouarar, I, Chabrillat, S, Crepulja, M, Engelen, RJ, Eskes, H, Flemming, J, Gaudel, A, Hendrick, F, Huijnen, V, Jones, L, Kapsomenakis, J, Katragkou, E, Keppens, A, Langerock, B, de Mazière, M, Melas, D, Parrington, M, Peuch, VH, Razinger, M, Richter, A, Schultz, MG, Suttie, M, Thouret, V, Vrekoussis, M, Wagner, A, Zerefos, C. 2015. Data assimilation of satellite retrieved ozone, carbon monoxide and nitrogen dioxide with ECMWF's Composition-IFS. *Atmospheric Chemistry and Physics* **15**: 5275–5303. DOI: http://dx.doi.org/10.5194/acp-15-5275-2015.

Kaiser, JW, Heil, A, Andreae, MO, Benedetti, A, Chubarova, N, Jones, L, Morcrette, J-J, Razinger, M, Schultz, MG, Suttie, M, van der Werf, GR. 2012. Biomass burning emissions estimated with a Global Fire Assimilation System based on observed fire radiative power. *Biogeosciences* **9**: 527–554. DOI: http://dx.doi.org/10.5194/bg-9-527-2012.

Laeng, A, Eckert, E, von Clarmann, T, Kiefer, M, Hubert, D, Stiller, G, Glatthor, N, López-Puertas, M, Funke, B, Grabowski, U, Plieninger, J, Kellmann, S, Linden, A, Lossow, S, Babenhauserheide, A, Froidevaux, L, Walker, K. 2018. On the improved stability of the version 7 MIPAS ozone record. *Atmospheric Measurement Techniques* **11**: 4693–4705. DOI: http://dx.doi.org/10.5194/amt-11-4693-2018.

Lefever, K, van der AR, Baier, F, Christophe, Y, Errera, Q, Eskes, H, Flemming, J, Inness, A, Jones, L, Lambert, J-C, Langerock, B, Schultz, MG, Stein, O, Wagner, A, Chabrillat, S. 2015. Copernicus stratospheric ozone service, 2009–2012: Validation, system intercomparison and roles of input data sets. *Atmospheric Chemistry and Physics* **15**: 2269–2293. DOI: http://dx.doi.org/10.5194/acp-15-2269-2015.

Livesey, NJ, Read, WG, Wagner, PA, Froidevaux, L, Lambert, A, Manney, GL, Millán, LF, Valle, HC, Pumphrey, ML, Santee, MJ, Schwartz, SW, Fuller, RA, Jarnot, RF, Knosp, BW, Martinez, E, Lay, RR. 2018. Version 4.2x Level 2 data quality and description document. Technical report. Jet Propulsion Laboratory. Available at http://mls.jpl.nasa.gov/. Accessed 4 May 2021.

Mueller, R, Träger-Chatterjee, C. 2014. Brief accuracy assessment of aerosol climatologies for the retrieval of solar surface radiation. *Atmosphere* **5**(4): 959–972. DOI: http://dx.doi.org/10.3390/atmos5040959.

Nédélec P, Blot, R, Boulanger, D, Athier, G, Cousin, J-M, Gautron, B, Petzold, A, Volz-Thomas, A, Thouret, V. 2015. Instrumentation on commercial aircraft for monitoring the atmospheric composition on a global scale: The IAGOS system, technical overview of ozone and carbon monoxide measurements, MOZAIC-IAGOS special issue. *Tellus B* **67**: 27791. DOI: http://dx.doi.org/10.3402./tellusb.v67.27791.

NOAA El Niño. Available at http://origin.cpc.ncep.noaa.gov/products/analysis_monitoring/ensostuff/ONI_v5.php. Accessed 4 May 2021.

Ordóñez, C, Elguindi, N, Stein, O, Huijnen, V, Flemming, J, Inness, A, Flentje, H, Katragkou, E, Moinat, P, Peuch, V-H, Segers, A, Thouret, V, Athier, G, vanWeele, M, Zerefos, CS, Cammas, J-P, Schultz, MG. 2010. Global model simulations of air pollution during the 2003 European heat wave. *Atmospheric Chemistry and Physics* **10**: 789–815. DOI: http://dx.doi.org/10.5194/acp-10-789-2010.

Park, S, Son, SW, Jung, MI, Park, J, Park, SS. 2020. Evaluation of tropospheric ozone reanalyses with independent ozonesonde observations in East Asia. *Geoscience Letters* **7**: 12. DOI: http://dx.doi.org/10.1186/s40562-020-00161-9.

Petzold A, Thouret, V, Gerbig, C, Zahn, A, Brenninkmeijer, CAM, Gallagher, M, Hermann, M, Pontaud, M, Ziereis, H, Boulanger, D, Marshall, J, Nédélec, P, Smit, HGJ, Friess, U, Flaud, J-M, Wahner, A, Cammas, J-P, Volz-Thomas, A. 2015. Global-scale atmosphere monitoring by in-service aircraft current achievements and future prospects of the European Research Infrastructure IAGOS. *Tellus B* **67**: 28452. DOI: http://dx.doi.org/10.3402/tellusb.v67.28452.

Polo, J, Alonso-Abella, M, Ruiz-Arias, A, Balenzategui, JL. 2017. Worldwide analysis of spectral factors for seven photovoltaic technologies. *Solar Energy* **142**: 194–203. DOI: http://dx.doi.org/10.1016/j.solener.2016.12.024.

Richter, A, Begoin, M, Hilboll, A, Burrows, JP. 2011. An improved NO_2 retrieval for the GOME-2 satellite instrument. *Atmospheric Measurement Techniques* **4**: 1147–1159. DOI: http://dx.doi.org/10.5194/amt-4-1147-2011.

Richter, A, Burrows, JP, Nüß, H, Granier, C, Niemeier, U. 2005. Increase in tropospheric nitrogen dioxide over China observed from space. *Nature* **437**: 129–132. DOI: http://dx.doi.org/10.1038/nature04092.

Schere, K, Flemming, J, Vautard, R, Chemel, C, Colette, A, Hogrefe, C, Bessagnet, B, Meleux, F, Mathur, R, Roselle, S, Hu, R-M, Sokhi, RS, Rao, ST, Galmarini, S. 2012. Trace gas/aerosol boundary concentrations and their impacts on continental-scale AQMEII modeling domains. *Atmospheric Environment* **53**: 38–50. DOI: http://dx.doi.org/10.1016/j.atmosenv.2011.09.043.

Sheese, PE, Walker, KA, Boone, CD, Bernath, PF, Froidevaux, L, Funke, B, Raspollini, P, von Clarmann, T. 2017. ACE-FTS ozone, water vapour, nitrous oxide, nitric acid, and carbon monoxide profile comparisons with MIPAS and MLS. *Journal of Quantitative Spectroscopy and Radiative Transfer* **186**: 63–80.

Sindelarova, K, Granier, C, Bouarar, I, Guenther, A, Tilmes, S, Stavrakou, T, Müller, J-F, Kuhn, U, Stefani, P, Knorr, W. 2014. Global data set of biogenic VOC emissions calculated by the MEGAN model over the last 30 years. *Atmospheric Chemistry and Physics* **14**: 9317–9341. DOI: http://dx.doi.org/10.5194/acp-14-9317-2014.

Sindelarova, KD. 2018. 81.3.1.1. Gridded speciated and total NMVOC emissions for the most recent year for

which meteorological fields are available. Issued by: CUNI/Katerina Sindelarova. Ref: CAMS81_2017SC1_ D81.3.1.1-201802_v1.odt CAMS81_2017SC1_D81.3. 1.1_201802_Emissions-CAMS-GLOB-BIO-2018. Available at https://atmosphere.copernicus.eu/sites/ default/files/2018-05/CAMS81_2017SC1_D81.3.1.1- 201802_v2_APPROVED_Ver2.pdf. Accessed 4 May 2021.

Smit, HGJ. 2013. *Quality assurance and quality control for ozonesonde measurements in GAW*. WMO/GAW No. 201. Geneva, Switzerland: World Meteorological Organisation.

Smit, HGJ, Straeter, BJ, Johnson, SJ, Oltmans, J, Davies, DW, Tarasick, B, Hoegger, R, Stubi, FJ, Schmidlin, T, Northam, AM, Thompson, JC, Witte, I. 2007. Boyd: Assessment of the performance of ECC-ozonesondes under quasi-flight conditions in the environmental simulation chamber: Insights from the Juelich Ozone Sonde Intercomparison Experiment (JOSIE). *Journal of Geophysical Research* **112**: D19306. DOI: http://dx.doi.org/10. 1029/2006JD007308.

Stein, O, Schultz, MG, Bouarar, I, Clark, H, Huijnen, V, Gaudel, A, George, M, Clerbaux, C. 2014. On the wintertime low bias of Northern Hemisphere carbon monoxide found in global model simulations. *Atmospheric Chemistry and Physics* **14**: 9295–9316. DOI: http://dx.doi.org/10.5194/acp-14-9295-2014.

Tørseth, K, Aas, W, Breivik, K, Fjæraa, AM, Fiebig, M, Hjellbrekke, AG, Lund Myhre, C, Solberg, S, Yttri, KE. 2012. Introduction to the European Monitoring and Evaluation Programme (EMEP) and observed atmospheric composition change during 1972–2009. *Atmospheric Chemistry and Physics* **12**: 5447–5481. DOI: http://dx.doi.org/10.5194/acp-12-5447-2012.

Val Martin, M, Heald, CL, Arnold, SR. 2014. Coupling dry deposition to vegetation phenology in the Community Earth System Model: Implications for the simulation of surface O₃. *Geophysical Research Letters* **41**: 2988–2996. DOI: http://dx.doi.org/10. 1002/2014GL059651.

Vrekoussis, M, Wittrock, F, Richter, A, Burrows, JP. 2010. GOME-2 observations of oxygenated VOCs: What can we learn from the ratio glyoxal to formaldehyde on a global scale? *Atmospheric Chemistry and Physics* **10**: 10145–10160. DOI: http://dx.doi. org/10.5194/acp-10-10145-2010.

Wagner, A, Blechschmidt, A-M, Bouarar, I, Brunke, E-G, Clerbaux, C, Cupeiro, M, Cristofanelli, P,

Eskes, H, Flemming, J, Flentje, H, George, M, Gilge, S, Hilboll, A, Inness, A, Kapsomenakis, J, Richter, A, Ries, L, Spangl, W, Stein, O, Weller, R, Zerefos, C. 2015. Evaluation of the MACC operational forecast system—Potential and challenges of global near-real-time modelling with respect to reactive gases in the troposphere. *Atmospheric Chemistry and Physics* **15**: 14005–14030. DOI: http://dx.doi. org/10.5194/acp-15-14005-2015.

Wang, Y, Ma, Y-F, Eskes, H, Inness, A, Flemming, J, Brasseur, GP. 2020. Evaluation of the CAMS global atmospheric trace gas reanalysis 2003–2016 using aircraft campaign observations. *Atmospheric Chemistry and Physics*. DOI: http://dx.doi.org/10.5194/ acp-20-4493-2020.

Williams, JE, van Velthoven, PFJ, Brenninkmeijer, CAM. 2013. Quantifying the uncertainty in simulating global tropospheric composition due to the variability in global emission estimates of Biogenic Volatile Organic Compounds. *Atmospheric Chemistry and Physics* **13**: 2857–2891. DOI: http://dx.doi.org/ 10.5194/acp-13-2857-2013.

Witte, JC, Thompson, AM, Smit, HGJ, Vömel, H, Posny, F, Stübi, R. 2018. First reprocessing of Southern Hemisphere ADditional OZonesondes profile records: 3. Uncertainty in ozone profile and total column. *Journal of Geophysical Research: Atmospheres* **123**: 3243–3268. DOI: http://dx.doi.org/10.1002/ 2017JD027791.

Wittrock, F, Richter, A, Oetjen, H, Burrows, JP, Kanakidou, M, Myriokefalitakis, S, Volkamer, R, Beirle, S, Platt, U, Wagner, T. 2006. Wagner, simultaneous global observations of glyoxal and formaldehyde from space. *Geophysical Research Letters* **33**: L16804. DOI: http://dx.doi.org/10.1029/ 2006GL026310.

WMO. 2013. WMO: Guidelines for the continuous measurements of ozone in the troposphere. GAW Report No. 209. Geneva, Switzerland: World Meteorological Organization.

Zeng, G, Williams, J, Fisher, J, Emmons, LK, Jones, N, Morgenstern, O, Robinson, J, Smale, D, Paton-Walsh, C, Griffith, D. 2015. Multi-model simulation of CO and HCHO in the Southern Hemisphere: Comparison with observations and impact of biogenic emissions. Faculty of Science, Medicine and Health — Papers: Part A. 2893. Available at https://ro.uow.edu.au/smhpapers/2893. Accessed 4 May 2021.